A new AMPK activator, GSK773, corrects fatty acid oxidation and differentiation defect in CPT2-deficient myotubes

Fatima-Zohra Boufroura[1], Carole Le Bachelier[1], Céline Tomkiewicz-Raulet[1], Dimitri Schlemmer[2], Jean-François Benoist[2], Pascal Grondin[3], Yann Lamotte[3], Olivier Mirguet[4], Sophie Mouillet-Richard[5], Jean Bastin[1] and Fatima Djouadi[1*]

[1]INSERM UMR-1124, Université Paris Descartes, Centre Universitaire des Saints Pères, 75006 Paris, France

[2]Hôpital Robert Debré, Centre de Référence des Maladies Héréditaires du Métabolisme, Service de Biochimie-Hormonologie, 75019 Paris, France

[3]Centre de Recherches François Hyafil, Laboratoires Oncodesign, 91140 Villebon-sur-Yvette, France

[4]Institut de Recherches Servier, 92150 Suresnes, France

[5]Université Sorbonne Paris Cité, INSERM UMR-S1147 MEPPOT, Centre Universitaire des Saints-Pères, Paris, France.

*To whom correspondence should be addressed at: INSERM UMR-1124, Université Paris Descartes, 45 rue des Saints Pères, 75006 Paris, France. Tel:+33 142862219; Fax: +33 142863868; Email: fatima.djouadi@inserm.fr

Abstract

Carnitine Palmitoyl Transferase 2 (CPT2) deficiency is one of the most common inherited fatty acid oxidation (FAO) defects and represents a prototypical mitochondrial metabolic myopathy. Recent studies have suggested a pivotal role of AMPK in skeletal muscle plasticity and mitochondrial homeostasis. Thus, we tested the potential of GSK773, a novel direct AMPK activator, to improve or correct FAO capacities in muscle cells from patients harboring various mutations.

We used control and patients' myotubes and studied parameters of fatty acid oxidation metabolism, of mitochondrial quantity and quality, and of differentiation. We found that AMPK is constitutively activated in patients' myotubes, which exhibit both reduced FAO and impaired differentiation. GSK773 improves or corrects several metabolic hallmarks of CPT2-deficiency (deficient FAO flux and C16-acylcarnitines accumulation) by up-regulating the expression of CPT2 protein. Beneficial effects of GSK773 are also likely due to stimulation of mitochondrial biogenesis and induction of mitochondrial fusion, by decreasing DRP1 and increasing MFN2. GSK773 also induces a shift in Myosin Heavy Chain isoforms toward the slow oxidative type and, therefore, fully corrects the differentiation process. We establish, through siRNA knockdowns and pharmacological approaches that these GSK773 effects are mediated through PGC-1α, ROS and p38 MAPK, all key players of skeletal muscle plasticity. GSK773 recapitulates several important features of skeletal muscle adaptation to exercise.

The results show that AMPK activation by GSK773 evokes the slow, oxidative myogenic program and triggers beneficial phenotypic adaptations in FAO-deficient myotubes. Thus, GSK773 might have therapeutic potential for correction of CPT2-deficiency.

Introduction

Several genetic defects are known to impact skeletal muscle functions and lead to myopathy. Among these disorders, metabolic myopathies refer to a sub-group of inherited metabolic diseases that share abnormalities of energy metabolism resulting in skeletal muscle dysfunction (1, 2). Since long-chain fatty acids are the major source of energy for skeletal muscle during sustained exercise or fasting, some mitochondrial fatty acid oxidation disorders are classified in metabolic myopathies. Carnitine Palmitoyl Tranferase 2 (CPT2), an enzyme located in the inner mitochondrial membrane, catalyzes with other proteins the entry of long chain FA into the mitochondria. CPT2 deficiency, a prototypical metabolic myopathy, is one of the most common FAO disorders and can present various phenotypes, the most frequent being the adult-onset form characterized by myalgia, stiffness, cramps, rhabdomyolysis and exercise intolerance (3). The therapy of these inherited diseases mainly consists of dietary recommendations, in absence of available drug therapy to date.

Human skeletal muscles are composed of different fiber types with specific properties depending on the functional demands, age and gender (4). One key criterion of fiber types classification is the protein expression of myosin heavy chain (MHC) isoforms. Hence, human muscle fibers express three isoforms of MHC: MHC-I, MHC-IIA and MHC-IIX, which are associated with muscle fiber phenotypes. The muscle fibers that express MHC-I are defined as "slow-twitch" based on the contractile properties, fatigue resistant and oxidative, based on their high mitochondrial content and reliance on oxidative metabolism. The fibers that express MHC-IIA and MHC-IIX are fast-twitch, with intermediate (glycolytic and oxidative) and glycolytic metabolism respectively; and are associated with lower mitochondrial content and low resistance to fatigue.

It is now widely acknowledged that skeletal muscle is a dynamic tissue with remarkable plasticity, in functional adaptation and remodeling in response to various stimuli such as strength and endurance training, cold exposure, nutritional and hormonal modifications, one of the best-studied being physical exercise (5, 6). For instance, endurance exercise-induced adaptations are reflected by changes in metabolic and contractile properties characterized by fiber type transformation and stimulation of mitochondrial oxidative metabolism. Complex and intricate networks regulate skeletal muscle plasticity. Over the last two decades, many signaling pathways and underlying molecular mechanisms responsible for skeletal muscle malleability have begun to be deciphered (5-7). Among the diverse regulators of mitochondrial biogenesis stimulation, fiber-type transformation and skeletal muscle metabolism reprogramming that have been identified features the AMPK (AMP activated protein kinase) (5, 6, 8, 9).

While mainly known as a cellular sensor of metabolic stress and energy deprivation, AMPK is also activated by contractile activity in skeletal muscle and, interestingly has recently emerged as a master player in skeletal muscle plasticity (8). Indeed, AMPK has been shown to regulate the expression and activity of the central downstream element of the signaling cascade involved in skeletal muscle plasticity, namely the peroxisome proliferator-activated receptor gamma co-activator 1-alpha (PGC-1α) (6, 7). PGC-1a acts as a transcriptional co-activator through recruitment of multiple transcription factors that regulate mitochondrial biogenesis and oxidative metabolism including peroxisome proliferator activated receptors (PPAR), nuclear respiratory factor 1 (NRF1) and NRF2, estrogen-related receptor a (ERRα), mitochondrial transcription factor A (Tfam) and type I fiber specification through myocyte enhancer factor 2 (MEF2) (10, 11). It is of note that overexpression of PGC-1α in skeletal muscle has been shown to induce both a mitochondrial biogenesis (12) and a shift in fiber types toward type I fibers (13). Thus, this co-activator integrates the main signaling pathways involved in the skeletal muscle adaptability to various stimuli. PGC-1α expression is highly regulated at transcriptional and post-translational levels (14). Several binding sites for transcription factors, such as MEF2, PPAR, cAMP response element-binding protein (CREB) and activating transcription factor 2 (ATF2), are present in the PGC-1α promoter. Importantly, PGC-1α interacts with MEF2, PPAR and CREB on its own promoter and autoregulates its own expression in a feed-forward regulatory loop (15, 16).

Post-translational modifications (PTM) of PGC-1α, including phosphorylation, acetylation, ubiquitination and methylation have also been described (14). Interestingly, AMPK phosphorylates the transcription factor CREB (17), leading to stimulate PGC-1α transcription and is also known to enhance PGC-1α activity by the phosphorylation at threonine-177 and serine-538 (18). Hence, AMPK is acknowledged to be an important player in skeletal muscle plasticity mainly because it is a central regulator of PGC-1α (19).

Interestingly, recent studies have uncovered an important role of AMPK in various aspects of mitochondrial biology and homeostasis (20). Hence, in addition to the pivotal role of AMPK as a regulator of mitochondrial biogenesis, likely through its action on PGC-1α, much evidence now points to a specific regulation of key proteins involved in the shape and the quality of the mitochondrial network (20). For instance, direct activation of AMPK with small molecules, in absence of mitochondrial damages was shown to induce mitochondrial fission and the mitochondrial fission factor (MFF). MFF is a mitochondrial outer-membrane primary receptor for dynamin-related protein 1 (DRP1), an enzyme that catalyzes mitochondrial fission was identified as a novel substrate of AMPK (21). Finally, recent works have also suggested that autophagy, a process responsible for removal of dysfunctional cellular components, can also be an important player in skeletal muscle remodeling

(22-25). Autophagy is highly dynamic and tightly regulated and several studies have demonstrated that AMPK controls the autophagy machinery at different steps (20).

Altogether, these recent data uncovering a novel role of AMPK as a pivotal regulator of both skeletal muscle plasticity and mitochondrial biology suggest that AMPK might represent a potential therapeutic target for myopathies originating from a FAO defect. We thus surmised that CPT2 deficiency, a prototypical metabolic myopathy, might benefit from pharmacological activation of AMPK. We tested this hypothesis by studying the effects of a new direct AMPK activator, GSK773, on the metabolic and structural phenotype of CPT2-deficient myotubes. The data presented here report that GSK773 remarkably improves several impaired metabolic and structural parameters exhibited *ex vivo* by CPT2-deficient myotubes.

Results

GSK773 improves metabolic features of CPT2 deficiency

The GSK773 compound (Figure 1A), a quinolinone derivative (26), was developed as a direct AMPK activator (Figure S1A) by monitoring phosphorylation of the SAMS peptide using AMPK purified from rat liver. GSK773 also protects rat liver AMPK from de-phosphorylation (Figure S1B) as shown through *In vitro* de-phosphorylation assay (27). Finally, GSK773 was demonstrated to be a β1 selective AMPK activator using human recombinant heterotrimers (Figure S1C).

We anticipated that GSK773 might have a beneficial effect on fatty acid oxidation (FAO) flux. Thus, palmitate oxidation rates were first measured in dose-response experiments performed in control and in CPT2-deficient myotubes, which showed that the optimal concentration of GSK773 was 30µM in cells treated for 48h (Figure 1B). Indeed, GSK773 induced significant increases of FAO flux in a dose-dependent manner in all myotubes with a restoration of normal values in patients' cells at 30µM. Under these optimal conditions of cell treatment, we observed that the mild but significant FAO deficiency exhibited under basal conditions in all patient cell lines, ranging from -16% (Patient 4) to -23% (Patient 1) of control values, was fully corrected after treatment with GSK773 (+21% to +39%) (Figure 1C). We then performed western-blot analysis to assess the effect of GSK773 on CPT2 protein level. The amounts of CPT2 protein were significantly reduced in all patients' myotubes, from -50% in Patient 1 up to -88% in Patient 2, compared to control levels (Figure 1D). In response to GSK773, we monitored a significantly 1.4-fold increase in CPT2 protein in control cells as well as an induction of mutated CPT2 protein in patients' myotubes from 1.4-fold (Patient 1) to 1.9-fold (Patient 3). These results were confirmed by immunofluorescence experiments (Figure S1D) showing that the specific staining of CPT2 protein was much less intense in deficient myotubes and that the CPT2 signal intensity was enhanced after treatment with GSK773. Analysis of CPT2 gene expression indicated that the CPT2 mRNA pool measured in both controls and CPT2-deficient myotubes was slightly increased by GSK773 (1.2 to 1.3-fold) (Figure 1E).

In CPT2-deficient patients, C16 acylcarnitine accumulation in plasma (28) or in cell culture medium (29) is a biochemical hallmark of the disorder. Here, we found that GSK773 significantly decreased, thus alleviated (Figure 1F) the 5.7-fold (Patient 1) to 2.6-fold (Patient 4) accumulation of C16-acylcarnitines. However, with the exception of Patient 4, the levels of C16 acylcarnitines were not corrected to control values.

Altogether, GSK773 clearly corrected or improved several biochemical features of CPT2 deficiency in primary cultured human skeletal muscle myotubes.

GSK773 corrects impaired differentiation of CPT2-deficient myotubes

In the course of cell cultures, we noticed that, in addition to obvious defects of proliferation, the CPT2-deficient cells always seemed less differentiated than the controls. As already mentioned, skeletal muscle is composed of fibers, which are classified upon morphological, metabolic and contraction properties. It is now acknowledged that the differentiation of muscle cells is characterized by the appearance of proteins specific of mature myotubes such as the myosin heavy chains (MHC). Hence, in order to objectivize our observations, we chose to study the expression of MHC-I, expressed in "slow-twitch" fibers that characteristically exhibit slow contraction rates, high mitochondrial content, and oxidative metabolism, and that of MHC-IIA expressed in "fast-twitch" fibers that exhibit rapid contraction, lower mitochondrial content and intermediate (glycolytic/oxidative) metabolism.

First, western blot analysis showed significantly reduced amounts of both MHC-I and MHC-IIA in CPT2-deficient myotubes compared to controls (Figure 2A and 2B), consistent with the notion of an impaired differentiation process in patients' myotubes. Similar results were obtained using MF20 antibody, which recognizes most MHC isoforms. GSK773 remarkably increased the amount of MHC-I protein (Figure 2A), which was restored to control levels. In contrast, the compound tended to reduce the amount of MHC-IIA in both controls and patients (Figure 2B). Altogether, these results show that GSK773 induced an increase in the ratio of slow to fast MHCs (Figure 2C), indicating a shift in MHC isoforms toward the slow oxidative type. These data appeared fully consistent with mRNAs analysis, which revealed a marked increase in MYH7 (MHC-I) gene expression after treatment, while *MYH2* (MHC-IIA) transcripts were decreased (Figure 2 D), in both controls and patient 1. Patient 1 was subsequently often studied because it was representative of other CPT2-deficient patients. Immunofluorescence images also confirmed these findings (Figure 2E and 2F), showing a clear induction of MHC-I signal associated with a reduced MHC-II staining, in the treated myotubes. Finally, we calculated the fusion index (% of nuclei present in MHC-I positive myotubes), a well-admitted parameter to assess the extent of differentiation. As shown in Figure 2G, the myogenic fusion index was significantly decreased in patient 1 myotubes compared to controls, confirming an impaired commitment to terminal differentiation. Of note, the fusion index was restored to control values after treatment.

Next we monitored myoblast proliferation and differentiation using the xCELLigence technology. This non-invasive methodology allows in real-time the measurement of electrical impedance, which reflects the number of cells, cell size and morphology, and cell attachment quality. The impedance of electron flow caused by adherent cells is reported using a parameter termed Cell Index (CI), which thus quantifies the cell status. Hence, xCELLigence analysis further supported an impaired differentiation process in CPT2-deficient myotubes. Indeed,

the 8-day kinetics of real-time monitoring showed recorded profiles remarkably different between control and patient 1 (Figure 3A) and can be divided in two phases: proliferation and differentiation of the muscle cells. After seeding, the myoblasts were allowed to proliferate for 48h, and this resulted in a progressive increase in the 0-48h CI values, corresponding to increased cell number. As seen in Figure 3B, the 48h-Ci values were significantly lower in all the patients' cells compared to controls, indicating that the CPT2-deficient myoblasts proliferate slower. At the end of this proliferation stage, the growth media was replaced and the cells were induced to differentiate. In the controls, the Ci values greatly increased during the first two days of differentiation, which correspond to elongation and migration of myocytes. Then, the Ci markedly decreased due to the initiation of the fusion process to form multi-nucleated myotubes. The Ci values were calculated at key time points and, with the exception of patient 4, were always found to be significantly lower than in controls (Figure 3B); the greatest difference occuring at the peak values, around 4-4.5 days. Thus, monitoring by xCELLigence reliably quantified, by cell index values, the impaired differentiation process of patients' myotubes. We used confocal microscopy to illustrate and further validate the interpretation of these profiles (Figure S2A).

The xCELLigence profiles obtained in controls and patients prompted us to consider treating the cells during the proliferation and/or during the differentiation steps rather than treating differentiated myotubes for 48h only. Thus, in a first set of experiments we treated myoblasts 4 days before seeding in E-plates, and once again at the time of plating in the microwells (Figure S2B), (i.e. all along proliferation). As already observed, the cell index measured at the peak was significantly decreased in Patient 1 compared to control. Although the cell index was increased in both cell lines after 6 days of exposure to GSK773 (Figure S2C), this protocol of treatment failed to restore a normal Ci value in Patient 1. Therefore, in subsequent experiments, we also added GSK773 in the differentiation medium and treated the cells, for 4 additional days (Figure 3C). The resulting 10-day treatment with GSK773 induced a spectacular improvement in Patient 1 profile, leading to its normalization (Figure 3C and 3D). The beneficial effect of GSK773 on the differentiation of patient 1-derived myotubes was confirmed by immunofluorescence labeling of MHC I (Figure 3E). Finally, we showed that this protocol of 10 days of cell treatment also led to a complete correction of FAO flux (Figure 3F). Thus, we may conclude that the biochemical defect and the impaired differentiation process associated with CPT2 deficiency can be alleviated by GSK773, a new AMPK activator.

AMPK and PGC-1α relay the action of GSK773

In a next step, we sought to delineate the molecular mechanisms that could account for the beneficial effects of GSK773 on the metabolism and the differentiation process in one control and Patient 1 myotubes. Since GSK773 is an AMPK activator we first examined the phosphorylation level of AMPKα1 at T172, a classical marker of AMPK activation (Figure 4A, 4B and S3A), in response to the GSK compound. Surprisingly, we observed that in vehicle-treated cells, AMPK was 2- to 3-fold more phosphorylated in CPT2-deficient myotubes than in control cells. This suggests that under basal conditions, AMPK is constitutively activated in the patients' myotubes. After treatment, GSK773 clearly increased the phosphorylation of AMPK in control cells while, in patient myotubes, the additional phosphorylation failed to be statistically significant. However, the ratio of phospho-AMPK to AMPK indicated that GSK773 increases the phosphorylation of AMPK in both control and CPT2 myotubes (Figure 4C).

To determine whether AMPK activation was required for the observed effects of GSK773, we evaluated the effects of AMPKα1 subunit silencing on the expression of CPT2 and MHCI proteins (Figure 4D-F). In human skeletal muscles, AMPKα1 and AMPKα2 subunits are both highly expressed (30, 31). Results shown below are for AMPKα1 silencing, similar results were obtained for AMPKα2 silencing (data not shown). As shown in Figures 4D and 4F, AMPKα1 silencing fully abrogated the GSK773-dependent induction of MHC-I in controls or patient 1 myotubes. This also holds true for CPT2 in both cell lines; however, there was still a slight but non-significant increase in CPT2 protein in treated myotubes, suggesting possible contributions of other signaling circuits to CPT2 induction. Interestingly, in Patient 1 myotubes (Figure 4E), we found that AMPK silencing *per se* induced a significant increase in CPT2 levels, which suggests that AMPK might have an inhibitory effect, at basal level. CPT2 protein levels appeared unaffected by AMPK silencing in control myotubes.

To evaluate whether the key transcriptional co-activator PGC-1α participates to the action of GSK773, we silenced the expression of PGC-1α using siRNAs. Recent works from different laboratories have shown that PGC-1α gene is controlled by two promoters, which give rise to different transcripts subjected to alternative splicing encoding several PGC-1α isoforms (32). Analysis of whole cell extracts using a monoclonal antibody revealed several bands at different molecular weights (Figure S3B-C) including the expected PGC-1α band at ≈ 100kDa. Interestingly, several of these bands, at already reported molecular weights for PGC-1α (32), appeared to be up-regulated by GSK773. We focused our attention on the canonical form of PGC-1α (≈ 100kDa) and the N-truncated form of (≈ 35kDa) proposed to play an important role in skeletal muscle (33-35).

As shown in Figure S3B-C the increases in both PGC-1α isoforms triggered by GSK773 were totally abolished by PGC-1α siRNA, and 4 days after siRNA transfection there were still low but detectable levels of PGC-1α proteins. These apparently intriguing results could be explained in light of the existence of an auto-regulatory feed-forward loop of PGC-1α regulation and of compensatory mechanisms due to the disruption of PGC-1α. More importantly, we checked that the expression of most PGC-1α isoforms including the canonical and the truncated forms were almost totally abolished 2 days after transfection, i.e when the treatment with GSK773 was applied to the myotubes (Figure S3D). We then assessed the effects of PGC-1α silencing on the two read-outs: CPT2 and MHC-I protein levels (Figure 4G-I). As already observed for AMPKα1, transfection of PGC-1α siRNA totally canceled the increases of MHCI in both controls and patient 1 (Figure 4I). Concerning CPT2 protein, although the increases induced by GSK773 were hampered by the PGC-1α siRNAs in both controls and patient 1, a slight but non-significant increase persisted (Figure 4H), suggesting the intervention of other signaling mechanisms. Collectively, these data suggest that PGC-1α contributes to the action of GSK773.

GSK773 induces a mild ROS production, which participates with p38MAPK to CPT2 and MHC-I induction.

Oxidative stress presumably produced by impaired mitochondrial metabolism has been proposed to play a detrimental role in some fatty acid oxidation disorders (36). Hence, we measured ROS generation in all cell lines (Figure 5A). Surprisingly, we found that ROS levels were significantly down-regulated in all CPT2-deficient myotubes compared to controls and that GSK773 led to a 1.6- to 2-fold increase in ROS, restoring the levels close to normal values (Figure 5A-B). Beyond yielding oxidative stress, it is now acknowledged that ROS, at least within certain concentrations, could have a positive role and serve as signaling molecules in muscle cells in physiological processes such as exercise (37). Interestingly, one of the major signaling pathways activated by exercise-induced ROS is the p38 mitogen-activated protein kinase (p38-MAPK), which incidentally has also been shown to regulate PGC-1α at both transcriptional and posttranslational levels (14). For instance, in skeletal muscle, p38 MAPK phosphorylates and activates the transcription factors MEF2 and ATF2, thereby inducing PGC-1α transcription. It also directly phosphorylates three residues on PGC-1α protein leading to its activation.

This led us to assess the ability of GSK773 to activate the p38-MAPK pathway in primary human myotubes. 48h-treatment was found to increase p38 phosphorylation in both controls and CPT2 patients (figure 5C-E and S4A). To further investigate the molecular mechanisms underlying the effects of GSK773 and test the putative involvements of ROS and p38-MAPK, we used the well-known antioxidant, N-acetyl-cysteine (NAC) and the

classical p38-MAPK inhibitor SB203580 in conjunction with GSK773. CPT2 and MHCI protein levels were again used as readouts (Figure 5F-5H). The removal of ROS by NAC (figure S4B) or the addition of the p38MAPK inhibitor both prevented the increases of CPT2 protein in controls and deficient cells triggered by GSK773 (Figure 5G). We also repeatedly measured higher CPT2 protein levels in control myotubes in the presence of NAC, suggesting a detrimental role of ROS in these cells, which will require further investigations. The results were quite different concerning the MHCI (Figure 5H). Indeed, the addition of NAC remarkably decreased the MHCI levels below the levels measured in vehicle-treated cells, and cancelled the effect of GSK773 in both control and patient-derived myotubes. The inhibition of p38 MAPK activity by SB203580 also impeded the effect of GSK773 in controls and Patient 1 myotubes (Figure 5H). As whole, the data suggest that ROS and p38 MAPK participate to the signaling cascade of GSK773.

GSK773 induces mitochondrial biogenesis and improves mitochondrial network quality.

The above results indicate that several PGC-1α isoforms were up-regulated by GSK773. Since this co-activator is well-known to stimulate mitochondrial biogenesis, we asked whether a mitochondrial biogenesis occurred in response to GSK773 treatment. Mitochondrial biogenesis is a complex and highly regulated process requiring, among others, the coordinate regulation of nuclear and mitochondrial genomes. Beyond CPT2, we found that citrate synthase protein, a commonly used marker of mitochondrial density, encoded by nuclear DNA, was also up-regulated (+25%) by GSK773 (Figure 6A). We next examined the mitochondrial transcription factor A (Tfam) encoded by the nuclear genome, and known to regulate the transcription and the replication of mitochondrial DNA. Tfam has also been shown to co-localize with mtDNA in the mitochondrial nucleoids and thus presumably reflects mtDNA copy number (38). As shown in Figure 6B, GSK773 markedly increased (1.7-fold) the amount of Tfam, which likely accounted for the increase in COX2 protein, a mtDNA-encoded subunit of complex IV. Altogether, these data support the view that GSK773 induces a mitochondrial biogenesis.

Recent studies have revealed that in addition to its well-known role as an energy metabolic sensor, AMPK might also be a key regulator of mitochondrial homeostasis, notably through the regulation of mitochondrial fission (39). We took advantage of CPT2 labeling to look more precisely at the mitochondrial morphology after 10 days treatment. As anticipated, the fluorescence staining was less intense in patient 1 in agreement with the CPT2 deficiency (Figure 6C). After GSK773 treatment, the CPT2 fluorescence intensity was greatly increased, and the mitochondrial network appeared more organized and elongated in myotubes. This was confirmed at higher magnification (Figure 6D). In patient 1, the mitochondrial network appeared fragmented and punctated

compared to control, which is known to be an indication of mitochondrial dysfunction. After GSK773 treatment, the network became substantially elongated, which is known to be an indication of healthier mitochondria. The machinery involved in mitochondrial dynamics requires several proteins including mitofusin 2 (MFN2), which participates to the fusion of mitochondria, and DRP1, which is involved in the fission. We assessed the expression of both proteins in response to GSK773 treatment (Figure 6E-6F). Interestingly, we showed that DRP1 expression was up-regulated at basal level in patient 1, and that 48 h of GSK773 treatment restored control levels (Figure 6E). In line with these results, we found that MFN2 protein levels were significantly increased after treatment (Figure 6F), mirroring mitochondrial fusion. Hence, our data argue that GSK773 improves the quality of the mitochondrial network.

GSK773 regulates autophagy

Recent data have suggested that AMPK also regulates autophagy, a process that might participate to skeletal muscle adaptation to various situations, in particular to exercise (22-25). During autophagy, damaged materials are sequestered in autophagosomes in a process where the microtubule-associated protein 1 light chain 3 (LC3-I) is lipidated to form the autophagosomes associated protein LC3-II. Thus, the content of LC3-II is considered a reliable indicator of autophagy under most conditions. We evaluated LC3-I and LC3-II isoforms by immunoblots and Figure 7 shows that CPT2-deficient myotubes exhibited an increased level of autophagy proteins (LC3-I + LC3-II, and LC3-II) compared to controls, suggesting an increase in autophagosome content. In control cells, GSK773 significantly increased (2.3-fold) the amount of LC3-II protein with no change in LC3-I protein (figure S4C). In CPT2-deficient myotubes, treatment with GSK773 resulted in a trend towards increased LC3-II (≈+30%) and LC3-I (≈+19%) protein levels in 3 out of 4 patients (Figure 7 and S4C). Thus, GSK773 appears to enhance autophagy, which may contribute to its positive action on myotube differentiation.

Discussion

AMPK has long been known to be a fuel sensor activated by the low energy status of the cells. The pleiotropic actions of this kinase in various tissues have boosted since many years the research on AMPK as a therapeutic target for common metabolic diseases, and the quest of new activators of AMPK as therapeutic drugs. However, recent advance in research on AMPK has expanded its actions and revealed new pivotal roles in both skeletal muscle plasticity (8) and mitochondrial homeostasis (20).

In this study, the use of primary human CPT2-deficient myotubes has proven to be a fruitful model system since it revealed not only expected hallmarks of the genetic defect (decreased FAO flux and C16-acylcarnitines accumulation) but also an unexpected but relevant defect in differentiation (decreased MHC-I and MHC-II abundance, abnormal xCELLigence profiles). We showed that treatment with the new direct AMPK activator GSK773 corrected the FAO defect and alleviated the C16-acylcarnitines toxic accumulation. It should be recalled that in the muscular form of CPT2 deficiency, the patient cells exhibit residual long-chain FAO capacities, which can be enhanced by various pharmacological treatments (40). In the present study, we found that relatively modest increases in CPT2 mutant mRNA and protein were sufficient to fully correct FAO flux as already observed, in some patient' cells treated with bezafibrate (41, 42) or resveratrol (43). For these compounds, distinct metabolic signaling pathways account for the beneficial effects on FAO flux. Indeed, bezafibrate, a hypolipidemic drug, is known to act as a direct activator of the nuclear receptor PPAR delta (44, 45), whereas resveratrol, a natural plant polyphenol, can activate sirtuin 1 (SIRT1) (43), estrogen receptor (ER) and ERRα (46). The mechanism of action of GSK773, which directly activates AMPK, is clearly different. However, it is worth mentioning that resveratrol and GSK773 have in common to involve PGC-1α. Thus, mitochondrial β-oxidation is under control of multiple endogenous signaling mechanisms, and our data reinforce the view that targeted pharmacological interventions can efficiently correct basic aspects of CPT2 deficiency, which might open new perspectives for the treatment of patients.

GSK773 also increased MHC-I abundance, reflecting a shift toward a more oxidative phenotype, and corrected the xCELLigence profiles. Hence, we document for the first time that, in this prototypical metabolic myopathy, two main components of the skeletal muscle plasticity, i.e. metabolism and expression of myosin isoforms, were impaired, and were corrected by pharmacological activation of the druggable AMPK. Altogether, these results posit skeletal muscle plasticity as a potential therapeutic approach for the treatment of metabolic myopathy.

Interestingly, we think that the unexpected differentiation defect of patient muscle cells uncovered in this study might explain some aspects of disease physiopathology. Indeed, follow-up of patients show that the clinical

manifestations of CPT2 deficiency include not only rhabdomyolysis episodes, but also a recovery period following these episodes, during which patients physical capacities remain limited for a long period of time, and which is experienced as a major handicap by the patients (42). The mechanisms of muscle regeneration following rhabdomyolysis are known to rely on activation of satellite cells (muscle stem cells), which proliferate to give rise to myoblasts that then differentiate into muscle fibers in order to repair the muscle tissue damages. In this respect, the slowdown of myoblast proliferation and the impairment of myotube differentiation, as demonstrated in the present study for CPT2-deficient patients, might well interfere with the muscle repair process, and account for the long recovery period characteristic of this myopathy.

Unsurprisingly, the data revealed an involvement of AMPK in the signaling cascade, since the changes in CPT2 and MHC-I observed in response to GSK773 were abolished by the siAMPK. Our results also suggest that GSK773 promotes mitochondrial biogenesis since citrate synthase and CPT2, both encoded by nuclear DNA and COX2, encoded by mtDNA, as well as Tfam, a key regulator of mtDNA replication and transcription, were up-regulated in response to treatment. Finally, GSK773 also acts on the shape of mitochondrial network by inducing MFN2 and decreasing DRP1, which led to more fused mitochondria, an indication of healthier organelles.

Interestingly, we observed that AMPK is constitutively phosphorylated in CPT2-deficient myotubes but not in control myotubes, which likely reflects the metabolic stress existing in the patients' cells. We also found that in the patients' cells, the mitochondrial network appears more fragmented, in agreement with the increased amount of the mitochondrial fission protein DRP1. These results are in line with recent data, in human osteosarcoma cells, showing that after energy stress induced by inhibition of respiratory chain with rotenone or antimycin A, AMPK is phosphorylated and is required to mediate mitochondrial fission (21). Collectively, our results constitute the first demonstration that in "genetically-stressed" myotubes, the cells adapt to permanent metabolic defect by phosphorylating AMPK, which subsequently triggers the fission of the mitochondrial network and likely the degradation of defective mitochondria. This role of AMPK as a metabolic sensor mediating mitochondrial fragmentation in CPT2-deficient cells is further supported by the AMPK silencing experiments. Indeed, in patients' cells the suppression of AMPK up-regulated the CPT2 protein levels, clearly indicating a negative role of AMPK at basal level. Hence, our data perfectly support the recent notion proposed by several authors that AMPK is involved in various aspect of mitochondrial homeostasis in cells and can have a dual role by regulating both mitochondrial dynamics and mitochondrial biogenesis. Furthermore, our model brings new insight on the role of AMPK in mitochondrial homeostasis by showing that distinct phosphorylation events dictate distinct fates for mitochondria. Indeed, it is well acknowledged that in situations of low cellular ATP

levels, AMP binds to the γ-subunit of AMPK subsequently enhancing its activity, while GSK773 binds to AMPK, specifically to the β1-subunit containing AMPK hetero-trimers and inhibits the dephosphorylation of Thr172 by protecting it from the action of phosphatases. It can therefore be surmised that these different AMPK phosphorylation processes somehow trigger distinct molecular events in the cells, leading either to mitochondria fragmentation or to mitochondrial fusion/biogenesis. In addition, our results indicate that the basal phosphorylation of AMPK in patients cells is not sufficient to trigger a mitochondrial biogenesis since the cells did not "self-correct" their metabolic deficiency. Indeed, only the activation of AMPK by GSK773 promotes an improvement of metabolic and structural parameters in CPT2-deficient-myotubes. How activations of AMPK on different subunits enable the stimulation of signaling pathways leading to different cellular fates is currently unknown and will need further investigation.

Autophagy is an important adaptive process by which the cells recycle macromolecules, proteins and organelles in responses to different forms of stress, using a machinery composed of multi-protein complexes catalyzing different steps (47). It is now acknowledged that the autophagic machinery is highly regulated, in particular by AMPK (20, 47). Our data suggest that, at basal level, CPT2-deficient myotubes, which can be considered as "stressed-cells", exhibit an increased content of autophagosomes, in agreement with the "hyper-phosphorylation" of AMPK and the fragmentation of the mitochondrial network, as discussed above. Thus, we document for the first time that CPT2 deficiency promotes autophagy at basal level. However, further research is obviously needed to study in detail autophagy/mitophagy in CPT2-deficient myotubes. Interestingly, GSK773 clearly induced autophagy in control myotubes, while a slighter induction was observed in CPT2-deficient cells. Taken together, our study suggests that GSK773-induced myotube adaptation likely requires both mitochondrial biogenesis and clearance of cellular components. Of note, this is in line with very recent papers showing that autophagy can occur concomitant with mitochondrial changes in skeletal muscle in response to contractile activity and exercise (23, 24).

Altogether, the beneficial effects of GSK773 on fatty acid oxidation and differentiation, showing a remodeling of CPT2-deficient myotubes toward a slower, more oxidative phenotype, appear to involve the master regulator of muscle plasticity, namely PGC-1α. Indeed, the transfection of myotubes with a mixture of PGC-1α siRNA prevented the increases in CPT2 and MHC-I triggered by GSK773. However, we had to take into account several technical considerations when assessing the possible involvement of PGC-1α in the signaling cascade of GSK773 and the role of possible post-translational modification (PTM) of PGC-1α. Indeed, as already mentioned, PGC-1α may undergo PTM such as phosphorylation by AMPK or p38-MAPK, and studies of these

PTM therefore appear very attractive (14). On another hand, recent studies have revealed the existence of multiple PGC-1α transcripts and protein isoforms originating from alternative promoter usage and/or alternative splicing (32), adding another layer of complexity in PGC-1α gene expression. However, the absence of commercial antibodies specific to phospho- PGC-1α and the difficulty to immunoprecipitate PGC-1α with subsequent assessment of phosho-residues in the context of multiple isoforms renders the experimental study of PTM quite complex. Nevertheless, we chose to try to study PGC-1α protein levels and that is why we have favored immunoblotting from total cellular extracts that detected many novel PGC-1α isoforms. The current investigations showed that several of these isoforms, the full-length PGC-1α and many smaller proteins, appeared increased by GSK773, likely due to the existence of a positive autoregulatory loop. Thus, building on these observations, we propose that GSK773 promotes PGC-1α activation through phosphorylation, and that subsequent co-activation of different transcription factors present on its promoter such as PPAR, CREB or MEF2 leads to increase PGC-1α gene transcription and PGC-1α protein levels. It is noteworthy that physical exercise has been shown to induce both the full length and the truncated forms (NT- PGC-1α and PGC-1α4) of PGC-1α in skeletal muscle (33, 34).

Reactive oxygen species (ROS) have long been considered to be deleterious species to skeletal muscle and even to play a causal and detrimental role in the pathology of many muscle diseases or conditions such as Duchenne Muscular Myopathy (DMD), muscular dystrophies or sarcopenia (48). Excessive ROS production has also been proposed to participate to the physiopathology of some fatty acid oxidation disorders (36). However, the most recent literature also agrees that at low levels ROS could play a positive role and could be an important player in skeletal muscle signaling (37, 49). Hence, it is now widely accepted that ROS act in a hormetic fashion (50). One important unexpected observation of our study is that at basal levels, CPT2 myotubes produced less ROS than control cells. Interestingly, since low levels of ROS are present in myotubes with impaired differentiation process, this led us to hypothesize that this might be causal. This assumption is supported by the fact that addition of the antioxidant NAC in control myotubes for 48h, which reduced ROS below normal values, decreased MHC-I abundance. Collectively, our results suggest that, in some metabolic myopathies oxidative stress is not a hallmark, in contrast to what is observed in others myopathies such as DMD (51, 52) in which the contribution of oxidative stress to the pathology in widely recognized and, in which antioxidant treatments is proposed as therapy.

Recently, ROS have been recognized to play important roles in skeletal muscle plasticity and it has long been established that muscle contractions during exercise lead to increased levels of ROS (6). Our findings show that

GSK773 induces a significant increase of ROS in control and CPT2 myotubes, restoring normal ROS levels in patients' cells. Mechanistically, we show that the increases of CPT2 and MHC-I triggered by GSK773 are hampered by concomitant treatment with the antioxidant NAC, supporting the notion that the GSK773-induced ROS production participates to the signaling cascade. The transduction of ROS signal in phenotypic and metabolic adaptations of skeletal muscle to various stimuli was reported to involve the activation of several kinases: the extracellular-regulated kinase (ERK1/2), c-jun N-terminal kinase (JNK) and p38 mitogen-activated protein kinase (p38 MAPK). We chose to study p38 MAPK because this kinase is proposed to play a pivotal role in skeletal muscle plasticity by increasing the activity of PGC-1α by several means (14). Indeed, p38 MAPK phosphorylates transcription factors regulating PGC-1α gene, such as ATF2 and MEF2, and directly phosphorylates PGC-1α itself. The suppression of the GSK773-induced increases in CPT2 and MHC-I by the classical p38 inhibitor SB203580 argues that p38 MAPK is a downstream relay of the ROS signal.

A schematic model of GSK773-induced CPT2 and MHC-I up-regulations is shown Figure 5I. We propose that GSK773, by increasing the phosphorylation level of AMPK directly and of p38 MAPK indirectly, activates PGC-1α at transcriptional and post-translational levels, which, in turn, accounts for the phenotypic adaptation of the myotubes reflected by the up-regulation of mitochondrial FAO and biogenesis, and the shift in MHC isoforms.

In conclusion, this study brings new data indicating that the direct AMPK activator GSK773 can be beneficial for the improvement of several hallmarks of CPT2 deficiency. More generally, our data confirmed recent studies, which underlie the crucial role of AMPK in skeletal muscle plasticity and mitochondrial homeostasis, but also brings new insight into the understanding of AMPK functions in muscle cells in a normal and pathophysiological context. Hence, our data show that AMPK, acting as a key regulator of mitochondrial biogenesis and slow, oxidative myogenic phenotype might be a relevant therapeutic target in certain pathophysiological conditions, especially those characterized by a FAO defect. Finally and interestingly, by acting not only on AMPK, but also on p38 MAPK and on ROS production, GSK773 evokes some key features of skeletal muscle adaptation to exercise.

Materials and Methods

Human primary culture

The human biological samples were sourced ethically and their research use was in accord with the terms of the informed consents under an IRB/EC approved protocol. The muscle biopsies were obtained in the course of a clinical trial (41, 42) and the primary skeletal muscle cells were isolated as described before (53). The characteristics of CPT2 patients are provided in Table 1. Myoblasts of healthy donors (n=4 controls) were obtained either from the research cells bank of AFM-Telethon or from muscle biopsies of patients that gave informed consent in the course of orthopedic surgery. All myoblasts used for the experiments were under passage 5. Myoblasts were cultured in Ham's F10 with Glutamax (GIBCO) containing 20% FBS 0.2% Ultroser G, 0.2% Primocin and 1mM Carnitine. To induce differentiation, myoblasts at 80-90% confluence were switched to DMEM with Glutamax (GIBCO) supplemented with 2% horse serum, 0.2% Primocin and 1mM Carnitine. Cells were cultured at 37°C at 5% CO_2.

Treatment

GSK773 (MW:396) was dissolved in DMSO to make a stock solution of 10mM, aliquoted and stored, protected from light at -20°C. Unless otherwise mentioned, the myotubes were treated for 48h, after 4 days of differentiation, with 30µM GSK773 or vehicle (DMSO).

RNA interference

Small interfering RNAs (siRNAs) targeting the AMPK or PGC-1α sequences and control non-target siRNAs were obtained from Dharmacon (ON-TARGET plus SMARTpool). On day 2 of differentiation, myotubes were transfected with 30nM AMPK siRNAs or 42,5nM PGC-1α siRNAs using Lipofectamine® RNAiMAX Reagent according to the manufacturer's instructions. The myotubes were then allowed to differentiate 2 more days, prior to treatment with 30µM GSK773 for 48h.

Fatty acid oxidation measurement

Fatty acid oxidation (FAO) measurements were determined by quantifying the production of $^{3}H_2O$ from (9,10-^{3}H) palmitate (Perkin Elmer). Myoblasts were plated at 3000 cells/well for controls or 5000 cells/well for CPT2 patients in 24-well gelatin coated plates and allowed to grow 3 days before refreshing the media and allowing the

growth for 3 more days. After 6 days of proliferation, the myoblasts were induced to differentiate for 4 days prior to treatment with GSK773 for 48h. For each individual, tritiated water release experiments were performed in triplicate (44). Myotubes were washed three times with Dulbecco's PBS and 200 µl (9,10(n)-3H) palmitic acid (60Ci/mmol) bound to fatty acid-free albumin (palmitate to BSA 1.3:1 molar ratio, final concentration 125 µM) and 1mM carnitine were added per well. Cells were incubated for 2 h at 37 C. After incubation, the mixture was removed and added to a tube containing 200 µl cold 10% trichloroacetic acid. The tubes were centrifuged10 min at 2200 g at 4°C and aliquots of supernatants (350µl) were removed, mixed with 55µl of 6M NaOH, and applied to ion-exchange resin. The columns were washed with 1,7 ml of water and the eluates were counted. Cell protein content was determined by the Lowry method. The oxidation rates were expressed as nmol of ^{3}H fatty acid oxidized per hour per mg of cell protein (nmol ^{3}H FA/ h/ mg prot).

Acylcarnitine analysis

Electrospray ionization tandem mass spectrometry (MS-MS) was used to study acylcarnitine profiles in palmitate-loaded myotubes. The same timeline of cell culture and treatment as described for determination of FAO were performed. On day 4 of differentiation, the myotubes were treated with GSK773 in a differentiation medium containing palmitate bound to fatty acid-free albumin (palmitate to BSA 4:1 molar ratio, final concentration 200 µM;) and 400µM carnitine. Myotubes were cultured 48 h at 37°C, and the culture medium was collected and stored at -80°C until analysis. The values were expressed relative to protein content determined by the Lowry method (54).

Chemicals and reagents

Unlabeled Standard for acylcarnitine®, containing carnitine (C0), acetylcarnitine (C2), propionylcarnitine (C3), butyrylcarnitine (C4), isovalerylcarnitine (C5), octanoylcarnitine (C8), myristoylcarnitine (C14) and palmitoylcarnitine (C16) were purchased from Cambridge Isotope Laboratories (Tewksbury, MA, USA). Stable isotopes, MassChrom® Amino Acids and Acylcarnitines from Dried Blood/Non Derivatised, containing C0-Carnitine-D9 , C2-Carnitine-D3, C3-Carnitine-D3, C4-Carnitine-D3, C5-Carnitine-D9 , C5DC-Carnitine-D6 , C6-Carnitine-D3, C8-Carnitine-D3, C10-Carnitine-D3, C12-Carnitine-D3, C14-Carnitine-D3, C16-Carnitine-D3 were supplied by Chromsystem (Gräfelfing, Germany). Quality Controls containing C0, C5-DC, C8, C16, C18 carnitines were purchased from the national external quality control society of the Netherlands (SKML). Chemical reagents, including MS-grade ammonium acetate and formic acid were obtained from Sigma–Aldrich (St. Louis, MO, USA). MS-grade water was produced by Milli-Q Integral 3 Purification System (Millipores,

Guyancourt, France). MS-grade methanol and acetonitrile were purchased from VWR International (Radnor, PA, USA)

Standard solutions, calibration standards and quality control (QC)

Lyophilized calibrators and internal standards were respectively rehydrated by 5 ml and 10 ml of water:methanol (1:1; v/v). Standard working solution were prepared by diluting 10 fold the rehydrated standard solution in water:methanol (1:1; v/v) and stored at -20°C until used. A one point calibration curve was calculated for each analyte using duplicate of extraction of the standard. For other compounds that are not included in the lyophilized calibrator (e.g. hydroxy- unsaturated- and dicarboxylic- derivatives), quantification was calculated by isotopic dilution calculation using the internal standard with the nearest structure and retention time (Table 2).

Chromatography and mass spectrometry

The chromatographic system consisted of an Acquity UPLC I-Class system coupled to a Xevo-TQD tandem mass spectrometer manufactured by Waters (Waters, Milford, MA, USA). Optimum separation was achieved with an Acquity UPLC BEH HILIC column (100 mm × 2.1 mm, 1.7 µm) (Waters, Milford, MA, USA) using a gradient with solvent A 5 mM ammonium acetate and solvent B acetonitrile. The injection volume was 5 µl, the flow rate 0.5 mL/min and the column was set at 40°C. The binary LC solvent gradient was 10% A (0 min), 45% A (1 min) and then back to 10% A at 1.1 min for a total run time of 3 min. Ionization was performed with an electrospray ionization (ESI) source in positive mode. Source parameters were: drying gas (nitrogen) temperature 650°C, flow 1200 L/h, cone gas Flow (nitrogen) 20 L/h, ionization voltage 500 V. Detection was performed in the multiple reaction monitoring (MRM) mode. LC raw data and peak integration were analysed with MassLynx V4.2 software.

Optimizations of mass parameters (cone voltage and collision energy) were determined by LC/MS/MS for each compound of the calibrator. For other compounds that are not included in the lyophilized calibrator, cone voltage and collision energy were extrapolated using the values obtained for the nearest structural compound (supplementary Table 1).

Sample preparation

80 µL of acetonitrile were added to 20 µL of sample (patient, standard and controls) for proteins precipitation. Samples were then centrifuged 5 min at 10 000 g. 25 µL of supernatant were mixed with 25 µL of internal standard mixture and 200 µL of methanol. 5 µL were directly injected into the LC/MS system.

Method validation

The method was validated for selectivity, linearity, lower limit of quantification (LLOQ), accuracy and precision, extraction recovery, matrix effect and stability following the NF ISO15189 method validation recommendations.

Western blotting

Total proteins were extracted from myotubes in lysis buffer containing 50 mM Tris-HCl pH 8, 150 mM NaCl, 0,5% Nonidet P40, 0,25% sodium deoxycholate, 0,1% sodium dodecyl sulfate (SDS), 1mM de phenylmethylsulfonyl fluoride, 1x protease inhibitor cocktail, (Complete mini, Roche), 1x Phosphatase inhibitor cocktail (PhosSTOP, Roche), 10mM Nicotinamide. Protein concentration was determined by the Lowry method. Protein extracts (15-20µg) were resolved by 10% or 12% SDS-PAGE and transferred to PVDF membranes. Membranes were blocked with 5%milk or 5% BSA in 1x TBS-T for 1 h before incubation with primary antibodies either overnight at 4°C or 1h at room temperature. Immunoreactive bands were scanned by densitometry with a computerized video densitometer and the results were expressed as arbitrary units normalized to the amount of a-tubulin. Most of the time, blots were stripped using Antibody Stripping Buffer (Gene Bio-Application) according to the manufacturer's instructions and probed again. The following antibodies were used: rabbit polyclonal anti-CPT2 (Millipore), mouse monoclonal anti-a-tubulin (Sigma-Aldrich), rabbit polyclonal anti-citrate synthase (Abcam), mouse monoclonal anti-MYH2 (Santa Cruz), mouse monoclonal anti-myosin, Skeletal, Slow (Sigma-Aldrich), rabbit polyclonal anti-AMPKα1 (Cell Signaling), rabbit polyclonal anti-AMPKα2 (Cell Signaling), rabbit monoclonal anti-phospho-AMPK (Thr172) (Cell Signaling), mouse monoclonal anti- PGC-1α (Calbiochem), rabbit polyclonal anti-p38 MAPK (Cell Signaling), rabbit polyclonal anti-phospho-p38 MAPK (Thr180/Thr182) (Cell Signaling), rabbit monoclonal anti-DRP1 (Cell Signaling), mouse monoclonal anti-MFN2 (Abcam), rabbit polyclonal anti-LC3A/B (Cell Signaling).

RNA analysis

Total RNA was prepared using TRIzol reagent (Life Technologies) according to the manufacturer's protocol and treated with DNAse I (Ambion). cDNA was generated from 1µg of total RNA using M-MLV Reverse Transcriptase (Invitrogen) and quantified in triplicates on the 7900HT Fast Real-Time PCR system (Applied Biosystems) using Absolute qPCR SYBR Green ROX Mix (Thermo Scientific). The primer sequences are shown below:

CPT2-F: AGCCTCTCTTGAATGATGGCC

CPT2-R: GATAGGTACATATCAAACCAGGG

MYH2- F : TGATCACTGGAGAATCTGGTGC

MYH2-R : GATGAATTTACCAAAGCGAGAGG

MYH7-F : GACATGCTGCTGATCACCAACA

MYH7-R : CGCCTGTCAGCTTATACATGGA

RPL13A-F : AAGGTCGTGCGTCTGAAG

RPL13A-R : GAGTCCGTGGGTCTTGAG

TBP-F : CAAACCCAGAATTGTTCTCCTT

TBP-R : ATGTGGTCTTCCTGAATCCCT

The results were expressed as the relative quantification of a target gene transcript normalized to two housekeeping genes RPL13A and TBP, using the ΔΔCt method.

Measurement of cellular reactive oxygen species

Total levels of cellular ROS were measured using 2',7'-dichlorodihydrofluorescein-diacetate (H2DCFDA, Invitrogen). Experiments were performed in 24-wells in which myotubes were incubated with 1µM H2DCFDA in PBS for 30min at 37°C. Cells were subsequently washed with PBS, lysed in 250µl of 1M NaOH and transferred to a 96-well black plate for measurement of fluorescence intensity with a plate reader (infinite®M200, Tecan). The results were normalized to the amount of protein in each well.

Immunofluorescence and confocal microscopy

Myoblastes were plated on gelatin-coated coverslips in 6-wells plates and induced to differentiate. Myotubes were fixed in 4% paraformaldehyde for 20 min and then permeabilized for 3 min by 0.2% Triton in PBS solution. After rinsing, cells were pre-incubated in PBS containing 1% BSA and 0.3M Glycine for 30 min. Myotubes were incubated, 1h at room temperature, with the primary antibody diluted in PBS containing 1% BSA. Cells were washed three times in PBS/ 0.1% Tween and then incubated, 1h at room temperature, with secondary antibody anti-rabbit Alexa Fluor 546 and/or anti-mouse Alexa Fluor 488 (Life Technologies). Nuclei were stained with blue-fluorescent TO-PRO-3 (Invitrogen). Coverslips were washed and mounted in Dako mounting medium (Dako corporation). Images were acquired on a Carl-Zeiss LSM 510 META confocal microscope and analyzed with Zeiss LSM Image Browser software.

Electric impedance measurement

Myoblast proliferation and differentiation were examined using the xCELLigence Real-Time Cellular Analysis (RTCA) system (ACEA Biosciences, Inc). Myoblasts were trypsinized and seeded at 6000 cells per well in a volume of 0.2 ml on 16-well plates (E-plates) with microelectrodes on the bottom of each well. The optimal cell number per well to achieve the best myotube differentiation was determined through titration experiments.

Myoblasts were allowed to proliferate 48h and then differentiated by switching proliferation medium to differentiation medium. The impedance was monitored every 15 min for 192h at 37°C, 5% CO_2 and expressed as cell index (CI). In each experiment, duplicates of each individual were run. The data were analyzed using the RTCA software and were normalized to the impedance value of each well either at the beginning of the proliferation or at the beginning of the differentiation.

Rat liver enzymes purification

A partially purified rat liver AMPK fraction was prepared essentially as described in (55). Briefly, rat liver tissue was homogenized, adjusted with 6% polyethylene-glycol, centrifuged and finally purified with anion exchanger liquid chromatography. SAMS-phosphorylation assay was used to select AMPK containing fractions during the procedure.

AMPK enzymatic assays

SAMS-phosphorylation assay

Rat liver AMPK activity was determined by phosphorylation of the SAMS peptide (His-Met-Arg-Ser-Ala-Met-Ser-Gly-Leu-His-Leu-Val-Lys-Arg-Arg) essentially as described in (27, 55, 56). Assay conditions were 50µM ATP, 4µCi/mL [^{33}P]-ATP (Perkin Elmer), 50µM SAMS in 25µL reaction buffer (Tris 50mM pH7.4, Brij-35 0.02%, glycerol 10%, DTT 1mM and 1% final DMSO). Briefly, after 30min incubation at 30°C, reaction was stopped by addition of 100µL phosphoric acid at 150mM. Phospho-peptide was then quantified by filtration on phosphocellulose filters (Multiscreen plates MSPHN6B, Merck Millipore) and scintillation counting with Microbeta instrument (Perkin Elmer). Data were expressed as "% basal activity".

Z'-LYTE assay

The different human recombinant AMPK (Thermo Fisher Scientific) were used in a FRET assay format (Z-'LYTE Kinase assay – Thermo Fisher Scientific). Assay conditions were 100µM ATP, 2µM peptide (ThermoFisher Scientific #PV4645), 1% final DMSO in Z'-LYTE kinase buffer. Reaction was initiated by

addition of 0.2 to 0.8ng recombinant AMPK (depending on enzyme batches) and then incubated for 1-hour at 30°C. A further 1-hour incubation at 30°C after addition of the development reagent (ThermoFisher Scientific #PV3295) was performed. FRET signal was then measured with an Envision instrument (Perkin Elmer) and converted to "% peptide phosphorylation" according to Z'-LYTE given calculation procedure. Evaluation of GSK773 was carried out using concentration-response curve and EC_{50} calculation. Data shown are means of at least 3 independent measurements.

Rat liver AMPK-dephosphorylation assay

This assay took advantage of having a magnesium-dependent protein-phosphatase activity co-purified with rat liver AMPK. Briefly, reaction was started by addition of MgCl2 (5mM final) in 50mM TRIS to the rat liver fraction. After 30min incubation at 30°C, reaction was stopped by addition of EDTA (10mM final). Phospho-AMPK was then monitored by western-blot using anti Thr172-phospho-AMPK (Cell signaling). A condition with 10mM NaF was used as 100% phospho-AMPK control (no dephosphorylation). Western blot analysis was performed using LI-COR IRDye® IR Dye secondary antibodies and visualized using an Odyssey Infrared Imager (LI-COR Biotechnology). Quantification of results was performed using Odyssey software (LI-COR Biotechnology) and expressed as % of the signal obtained in NaF conditions.

Statistical analysis

The results are presented as the mean ± SD or ±SEM. Differences between groups were analyzed by paired or unpaired Student's *t* test for the comparison of two groups, or by one-way ANOVA and the Fisher test for comparison of three or more groups. GraphPad Prism 6 software was used. $P<0.05$ was considered significant.

Acknowledgements

We thank Alain Daugan for his contribution to GSK773 design and Florent Potvain and Eric Boursier for their technical support in AMPK enzymatic experiments. Olivier Biondi is acknowledged for his help in ROS immunofluorescence experiments.

Conflicts of interest statement. None declared

Funding

This work was supported by grants from the Association Française contre les Myopathies (AFM) and the Agence Nationale de la Recherche (ANR) and by INSERM. F.Z.B. was a recipient of a Cifre fellowship from GlaxoSmithKline.

References

1 Berardo, A., DiMauro, S. and Hirano, M. (2010) A diagnostic algorithm for metabolic myopathies. *Curr. Neurol. Neurosci. Rep.*, **10**, 118-126.

2 Smith, E.C., El-Gharbawy, A. and Koeberl, D.D. (2011) Metabolic myopathies: clinical features and diagnostic approach. *Rheum. Dis. Clin. North Am.*, **37**, 201-217.

3 Bonnefont, J.P., Djouadi, F., Prip-Buus, C., Gobin, S., Munnich, A. and Bastin, J. (2004) Carnitine palmitoyltransferases 1 and 2: biochemical, molecular and medical aspects. *Mol. Aspects. Med.*, **25**, 495-520.

4 Schiaffino, S. and Reggiani, C. (2011) Fiber types in mammalian skeletal muscles. *Physiol. Rev.*, **91**, 1447-1531.

5 Egan, B. and Zierath, J.R. (2013) Exercise metabolism and the molecular regulation of skeletal muscle adaptation. *Cell. Metab.*, **17**, 162-184.

6 Hoppeler, H. (2016) Molecular networks in skeletal muscle plasticity. *J. Exp. Biol.*, **219**, 205-213.

7 Kupr, B. and Handschin, C. (2015) Complex Coordination of Cell Plasticity by a PGC-1alpha-controlled Transcriptional Network in Skeletal Muscle. *Front. Physiol.*, **6**, 325.

8 Mounier, R., Theret, M., Lantier, L., Foretz, M. and Viollet, B. (2015) Expanding roles for AMPK in skeletal muscle plasticity. *Trends Endocrinol. Metab.*, **26**, 275-286.

9 Sanchez, A.M., Candau, R.B., Csibi, A., Pagano, A.F., Raibon, A. and Bernardi, H. (2012) The role of AMP-activated protein kinase in the coordination of skeletal muscle turnover and energy homeostasis. *Am. J. Physiol. Cell. Physiol.*, **303**, C475-485.

10 Handschin, C. and Spiegelman, B.M. (2006) Peroxisome proliferator-activated receptor gamma coactivator 1 coactivators, energy homeostasis, and metabolism. *Endocr. Rev.*, **27**, 728-735.

11 Scarpulla, R.C., Vega, R.B. and Kelly, D.P. (2012) Transcriptional integration of mitochondrial biogenesis. *Trends Endocrinol. Metab.*, **23**, 459-466.

12 Wu, Z., Puigserver, P., Andersson, U., Zhang, C., Adelmant, G., Mootha, V., Troy, A., Cinti, S., Lowell, B., Scarpulla, R.C. *et al.* (1999) Mechanisms controlling mitochondrial biogenesis and respiration through the thermogenic coactivator PGC-1. *Cell*, **98**, 115-124.

13 Lin, J., Wu, H., Tarr, P.T., Zhang, C.Y., Wu, Z., Boss, O., Michael, L.F., Puigserver, P., Isotani, E., Olson, E.N. *et al.* (2002) Transcriptional co-activator PGC-1 alpha drives the formation of slow-twitch muscle fibres. *Nature*, **418**, 797-801.

14 Fernandez-Marcos, P.J. and Auwerx, J. (2011) Regulation of PGC-1alpha, a nodal regulator of mitochondrial biogenesis. *Am. J. Clin. Nutr.*, **93**, 884S-890.

15 Handschin, C., Rhee, J., Lin, J., Tarr, P.T. and Spiegelman, B.M. (2003) An autoregulatory loop controls peroxisome proliferator-activated receptor gamma coactivator 1alpha expression in muscle. *Proc. Natl. Acad. Sci. U S A*, **100**, 7111-7116.

16 Schuler, M., Ali, F., Chambon, C., Duteil, D., Bornert, J.M., Tardivel, A., Desvergne, B., Wahli, W., Chambon, P. and Metzger, D. (2006) PGC1alpha expression is controlled in skeletal muscles by PPARbeta, whose ablation results in fiber-type switching, obesity, and type 2 diabetes. *Cell. Metab.*, **4**, 407-414.

17 Thomson, D.M., Herway, S.T., Fillmore, N., Kim, H., Brown, J.D., Barrow, J.R. and Winder, W.W. (2008) AMP-activated protein kinase phosphorylates transcription factors of the CREB family. *J. Appl. Physiol. (1985)*, **104**, 429-438.

18 Jager, S., Handschin, C., St-Pierre, J. and Spiegelman, B.M. (2007) AMP-activated protein kinase (AMPK) action in skeletal muscle via direct phosphorylation of PGC-1alpha. *Proc. Natl. Acad. Sci. U S A*, **104**, 12017-12022.

19 Canto, C. and Auwerx, J. (2010) AMP-activated protein kinase and its downstream transcriptional pathways. *Cell. Mol. Life Sci.*, **67**, 3407-3423.

20 Herzig, S. and Shaw, R.J. (2018) AMPK: guardian of metabolism and mitochondrial homeostasis. *Nat. Rev. Mol. Cell. Biol.*, **19**, 121-135.

21 Toyama, E.Q., Herzig, S., Courchet, J., Lewis, T.L., Jr., Loson, O.C., Hellberg, K., Young, N.P., Chen, H., Polleux, F., Chan, D.C. *et al.* (2016) Metabolism. AMP-activated protein kinase mediates mitochondrial fission in response to energy stress. *Science*, **351**, 275-281.

22 Fritzen, A.M., Madsen, A.B., Kleinert, M., Treebak, J.T., Lundsgaard, A.M., Jensen, T.E., Richter, E.A., Wojtaszewski, J., Kiens, B. and Frosig, C. (2016) Regulation of autophagy in human skeletal muscle: effects of exercise, exercise training and insulin stimulation. *J. Physiol.*, **594**, 745-761.

23 Ju, J.S., Jeon, S.I., Park, J.Y., Lee, J.Y., Lee, S.C., Cho, K.J. and Jeong, J.M. (2016) Autophagy plays a role in skeletal muscle mitochondrial biogenesis in an endurance exercise-trained condition. *J. Physiol. Sci.*, **66**, 417-430.

24 Kim, Y. and Hood, D.A. (2017) Regulation of the autophagy system during chronic contractile activity-induced muscle adaptations. *Physiol. Rep.*, **5**.

25 Lira, V.A., Okutsu, M., Zhang, M., Greene, N.P., Laker, R.C., Breen, D.S., Hoehn, K.L. and Yan, Z. (2013) Autophagy is required for exercise training-induced skeletal muscle adaptation and improvement of physical performance. *FASEB J.*, **27**, 4184-4193.

26 Daugan, A.C.-M., Lamotte, Y. and Mirguet, O. (2012) Patent WO 2012119978A1 Quinolinone derivatives as activators of AMPK. http://www.google.com.py/patents/WO2012119978A1?cl=en.

27 Sanders, M.J., Grondin, P.O., Hegarty, B.D., Snowden, M.A. and Carling, D. (2007) Investigating the mechanism for AMP activation of the AMP-activated protein kinase cascade. *Biochem. J.*, **403**, 139-148.

28 Carpenter, K.H. and Wiley, V. (2002) Application of tandem mass spectrometry to biochemical genetics and newborn screening. *Clin. Chim. Acta.*, **322**, 1-10.

29 Shen, J.J., Matern, D., Millington, D.S., Hillman, S., Feezor, M.D., Bennett, M.J., Qumsiyeh, M., Kahler, S.G., Chen, Y.T. and Van Hove, J.L. (2000) Acylcarnitines in fibroblasts of patients with long-chain 3-hydroxyacyl-CoA dehydrogenase deficiency and other fatty acid oxidation disorders. *J. Inherit. Metab. Dis.*, **23**, 27-44.

30 Jensen, T.E., Leutert, R., Rasmussen, S.T., Mouatt, J.R., Christiansen, M.L., Jensen, B.R. and Richter, E.A. (2012) EMG-normalised kinase activation during exercise is higher in human gastrocnemius compared to soleus muscle. *PLoS One*, **7**, e31054.

31 Nielsen, J.N., Mustard, K.J., Graham, D.A., Yu, H., MacDonald, C.S., Pilegaard, H., Goodyear, L.J., Hardie, D.G., Richter, E.A. and Wojtaszewski, J.F. (2003) 5'-AMP-activated protein kinase activity and subunit expression in exercise-trained human skeletal muscle. *J. Appl. Physiol. (1985)*, **94**, 631-641.

32 Martinez-Redondo, V., Pettersson, A.T. and Ruas, J.L. (2015) The hitchhiker's guide to PGC-1alpha isoform structure and biological functions. *Diabetologia*, **58**, 1969-1977.

33 Baar, K., Wende, A.R., Jones, T.E., Marison, M., Nolte, L.A., Chen, M., Kelly, D.P. and Holloszy, J.O. (2002) Adaptations of skeletal muscle to exercise: rapid increase in the transcriptional coactivator PGC-1. *FASEB J.*, **16**, 1879-1886.

34 Ydfors, M., Fischer, H., Mascher, H., Blomstrand, E., Norrbom, J. and Gustafsson, T. (2013) The truncated splice variants, NT-PGC-1alpha and PGC-1alpha4, increase with both endurance and resistance exercise in human skeletal muscle. *Physiol. Rep.*, **1**, e00140.

35 Zhang, Y., Huypens, P., Adamson, A.W., Chang, J.S., Henagan, T.M., Boudreau, A., Lenard, N.R., Burk, D., Klein, J., Perwitz, N. *et al.* (2009) Alternative mRNA splicing produces a novel biologically active short isoform of PGC-1alpha. *J. Biol. Chem.*, **284**, 32813-32826.

36 Olsen, R.K., Cornelius, N. and Gregersen, N. (2013) Genetic and cellular modifiers of oxidative stress: what can we learn from fatty acid oxidation defects? *Mol. Genet. Metab.*, **110 Suppl**, S31-39.

37 Powers, S.K., Duarte, J., Kavazis, A.N. and Talbert, E.E. (2010) Reactive oxygen species are signalling molecules for skeletal muscle adaptation. *Exp. Physiol.*, **95**, 1-9.

38 Kang, D., Kim, S.H. and Hamasaki, N. (2007) Mitochondrial transcription factor A (TFAM): roles in maintenance of mtDNA and cellular functions. *Mitochondrion*, **7**, 39-44.

39 Toyama, E.Q., Herzig, S., Courchet, J., Lewis, T.L., Jr., Loson, O.C., Hellberg, K., Young, N.P., Chen, H., Polleux, F., Chan, D.C. *et al.* (2016) Metabolism. AMP-activated protein kinase mediates mitochondrial fission in response to energy stress. *Science*, **351**, 275-281.

40 Bastin, J. (2014) Regulation of mitochondrial fatty acid beta-oxidation in human: what can we learn from inborn fatty acid beta-oxidation deficiencies? *Biochimie*, **96**, 113-120.

41 Bonnefont, J.P., Bastin, J., Behin, A. and Djouadi, F. (2009) Bezafibrate for treatment of an inborn mitochondrial ß-oxidation defect. *N. Engl. J. Med.*, **360**, 838-840.

42 Bonnefont, J.P., Bastin, J., Laforet, P., Aubey, F., Mogenet, A., Romano, S., Ricquier, D., Gobin-Limballe, S., Vassault, A., Behin, A. *et al.* (2010) Long-term follow-up of bezafibrate treatment in patients with the myopathic form of carnitine palmitoyltransferase 2 deficiency. *Clin. Pharmacol. Ther.*, **88**, 101-108.

43 Bastin, J., Lopes-Costa, A. and Djouadi, F. (2011) Exposure to resveratrol triggers pharmacological correction of fatty acid utilization in human fatty acid oxidation-deficient fibroblasts. *Hum. Mol. Genet.*, **20**, 2048-2057.

44 Djouadi, F., Aubey, F., Schlemmer, D. and Bastin, J. (2005) Peroxisome Proliferator Activated Receptor delta (PPARδ) Agonist But Not PPARα Corrects Carnitine Palmitoyl Transferase 2 Deficiency in Human Muscle Cells. *J. Clin. Endocrinol. Metab.*, **90**, 1791-1797.

45 Djouadi, F., Bonnefont, J.P., Thuillier, L., Droin, V., Khadom, N., Munnich, A. and Bastin, J. (2003) Correction of fatty acid oxidation in carnitine palmitoyl transferase 2-deficient cultured skin fibroblasts by bezafibrate. *Pediatr. Res.*, **54**, 446-451.

46 Lopes Costa, A., Le Bachelier, C., Mathieu, L., Rotig, A., Boneh, A., De Lonlay, P., Tarnopolsky, M.A., Thorburn, D.R., Bastin, J. and Djouadi, F. (2014) Beneficial effects of resveratrol on respiratory chain defects in patients' fibroblasts involve estrogen receptor and estrogen-related receptor alpha signaling. *Hum. Mol. Genet.*, **23**, 2106-2119.

47 Dikic, I. and Elazar, Z. (2018) Mechanism and medical implications of mammalian autophagy. *Nat. Rev. Mol. Cell. Biol.*, **19**, 349-364.

48 Guigas, B., Taleux, N., Foretz, M., Detaille, D., Andreelli, F., Viollet, B. and Hue, L. (2007) AMP-activated protein kinase-independent inhibition of hepatic mitochondrial oxidative phosphorylation by AICA riboside. *Biochem. J.*, **404**, 499-507.

49 Barbieri, E. and Sestili, P. (2012) Reactive oxygen species in skeletal muscle signaling. *J. Signal Transduct.*, **982794**, 1-17.

50 Ji, L.L., Kang, C. and Zhang, Y. (2016) Exercise-induced hormesis and skeletal muscle health. *Free Radic. Biol. Med.*, **98**, 113-122.

51 Kozakowska, M., Pietraszek-Gremplewicz, K., Jozkowicz, A. and Dulak, J. (2015) The role of oxidative stress in skeletal muscle injury and regeneration: focus on antioxidant enzymes. *J. Muscle Res. Cell. Motil.*, **36**, 377-393.

52 Moulin, M. and Ferreiro, A. (2017) Muscle redox disturbances and oxidative stress as pathomechanisms and therapeutic targets in early-onset myopathies. *Semin. Cell. Dev. Biol.*, **64**, 213-223.

53 Djouadi, F., Bonnefont, J.P., Munnich, A. and Bastin, J. (2003) Characterization of fatty acid oxidation in human muscle mitochondria and myoblasts. *Mol. Genet. Metab.*, **78**, 112-118.

54 Lowry, O.H., Rosebrough, N.J., Farr, A.L. and Randall, R.J. (1951) Protein measurement with the folin phenol reagent. *J. Biol. Chem.*, **193**, 265-275.

55 Carling, D., Clarke, P.R., Zammit, V.A. and Hardie, D.G. (1989) Purification and characterization of the AMP-activated protein kinase. Copurification of acetyl-CoA carboxylase kinase and 3-hydroxy-3-methylglutaryl-CoA reductase kinase activities. *Eur. J. Biochem.*, **186**, 129-136.

56 Davies, S.P., Carling, D. and Hardie, D.G. (1989) Tissue distribution of the AMP-activated protein kinase, and lack of activation by cyclic-AMP-dependent protein kinase, studied using a specific and sensitive peptide assay. *Eur. J. Biochem.*, **186**, 123-128.

Legends to figures

Figure 1. GSK773 improves fatty acid oxidation deficiency in human myotubes.

(A) Chemical structure of GSK773

(B) Dose-response studies of GSK773 effects on tritiated palmitate oxidation rates in control and CPT2 patients. The myotubes were treated for 48h; (n=4 different experiments, in each experiment, the determinations were performed in triplicate).

(C) b-oxidation flux measured in myotubes of controls (n=3) and CPT2 patients treated with 30 μM GSK773 or vehicle (DMSO) for 48h; (n=4-15 different experiments).

(D) Representative western blots and quantification of CPT2 protein (30 μM GSK773, 48h); (n=4-8 different experiments).

(E) CPT2 mRNA expression (30 μM GSK773, 48h); (n=3 different experiments).

(F) Quantification of C16:0 acylcarnitine production by tandem mass spectrometry (30 μM GSK773, 48h); (n=6-7 different experiments).

All data are means ± SEM. *p<0.05, **p<0.01, ***p<0.001, ****p<0.0001 compared with vehicle-treated myotubes; #p<0.05, ##p<0.01, ###p<0.001, ####p<0.0001 compared with control myotubes.

Figure 2. GSK773 induces a shift of MHC isoforms toward the slow oxidative type in human myotubes.

(A) Representative western blots and quantification of MHC-I protein in myotubes treated 30 μM GSK773, 48h; (n=3-6 experiments).

(B) Representative western blots and quantification of MHC-IIA protein; (n=3-6 experiments).

(C) MHC-I/MHC-IIA protein ratio

(D) MYH7 and MYH2 mRNA expression in 48h-treated myotubes; (n=3-4 experiments).

(E-F) Immunofluorescence images with antibodies against MHC-I (E) and MHC-II (F) in green, and Topro-3-labeled nuclei in blue.

(G) The fusion index, which is the number of nuclei present in myotubes divided by the total number of nuclei, was calculated. Two independent experiments were performed. Four fields of each condition were counted at x20 magnification.

Data are means ± SEM. *p<0.05, **p<0.01, ****p<0.0001 compared with vehicle-treated myotubes; #p<0.05, ##p<0.01, ###p<0.001, ####p<0.0001 compared with control myotubes.

Figure 3. GSK773 corrects the impaired differentiation process in CPT2-deficient myotubes.

(A) Representative kinetics of muscle cells during proliferation and differentiation using xCELLigence system.

(B) Histograms of cell index at different times; (n=6-10 experiments).

(C) Representative kinetics of muscle cells treated with 30µM GSK773 during proliferation and differentiation, the blue arrows represent the treatments.

(D) Maximum cell index of myotubes treated for 10 days; (n=3-4 experiments).

(E) Representative immunofluorescence images: MHC-I (green), CPT2 (red) and Topro-3-labeled nuclei (blue).

(F) Fatty acid oxidation flux measured in myotubes treated for 10 days; (n=3 experiments).

Data are means ± SEM. *p<0.05, **p<0.01 compared with vehicle-treated myotubes; #p<0.05, ##p<0.01, ###p<0.001, ####p<0.0001 compared with control myotubes.

Figure 4. AMPK is constitutively phosphorylated in CPT2 patients, and AMPK and PGC-1α are involved in signaling pathway triggered by GSK773.

(A) Representative western blots of AMPKα1 and P-AMPK (n=4-6 experiments).

(B) Quantification of P-AMPK protein levels in myotubes (30 µM GSK773, 48h).

(C) P-AMPK/AMPK protein ratio.

(D) Representative western blots of AMPKα1, CPT2 and MHC-I. Myotubes were transfected with siNon-target (NT) or siAMPKα1 at day 2 of differentiation, were allowed to differentiate 2 more days and were then treated with 30 µM GSK773 for 48h.

(E) Quantification of CPT2 protein levels in transfected myotubes (n= 3-4 independent experiments).

(F) Quantification of MHC-I protein levels in transfected myotubes (n= 3-4 independent experiments).

(G) Representative western blots of CPT2 and MHC-I from myotubes transfected with siNon-target (NT) or siPGC-1α, and treated with 30 µM GSK773 for 48h.

(H) Quantification of CPT2 protein levels in transfected myotubes (n= 5 independent experiments).

(I) Quantification of MHC-I protein levels in transfected myotubes (n= 3-5 independent experiments).

Data are means ± SEM. *p<0.05, **p<0.01, ***p<0.001 versus vehicle-treated myotubes; #p<0.05, ##p<0.01, ###p<0.001, ####p<0.0001 compared with control myotubes.

Figure 5. ROS and p38-MAPK are involved in signaling pathway triggered by GSK773.

(A) Relative measurement of total cellular reactive oxygen species (ROS) production in myotubes, after 48h of treatment with 30µM GSK773 (n=3 independent experiments).

(B) Representative fluorescence images of myotubes loaded with the ROS sensor CM-H2DCFDA.

(C) Representative western blots of p38-MAPK and P-p38-MAPK (n=3 different experiments).

(D) Quantification of P-p38 protein levels in myotubes (30 µM GSK773, 48h).

(E) P-p38/ p38 ratio

(F) Representative western blots of CPT2 and MHC-I from myotubes treated with 30µM GSK773 for 48h in conjunction with 10mM N-acetyl-cysteine (NAC) or 10µM SB203580 (myotubes were pre-treated with the p38 inhibitor 30min prior addition of GSK773).

(G) Quantification of CPT2 protein levels (n= 4 independent experiments).

(H) Quantification of MHC-I protein levels (n=4 independent experiments).

(I) Proposed schematic model of the effects of GSK773 on CPT2 and MHC-I.

Data are means ± SEM. *p<0.05, **p<0.01, ***p<0.001, ****p<0.0001 compared with vehicle-treated myotubes; #p<0.05, ####p<0.0001 compared with control myotubes.

Figure 6. GSK773 acts on mitochondrial biogenesis and on mitochondrial network.

(A) Quantification of citrate synthase protein levels in myotubes (30 µM GSK773, 48h); (n=6-9 experiments).

(B) Quantification of Tfam and COX2 protein levels; (n=3-6 experiments).

(C) Immunofluorescence images of 10 days-treated myotubes: CPT2 (red) and Topro-3-labeled nuclei (blue) at x40 magnification and (D) x80 magnification.

(E) Quantification of DRP1 protein levels in myotubes (30 µM GSK773, 48h); (n=4-6 experiments).

(F) Quantification of MFN2 protein levels in myotubes (30 µM GSK773, 48h); (n=5-6 experiments).

Data are means ± SEM. *p<0.05, **p<0.01, ***p<0.001, ****p<0.0001 compared with vehicle-treated myotubes; #p<0.05, ##p<0.01 compared with control myotubes.

Figure 7. GSK773 increases the content of autophagosomes.

(A) Representative western blots of LC3-I and LC3-II (n=3 different experiments).

(B) Quantification of LC3-I + LC3-II protein levels.

(C) Quantification of LC3-II protein levels.

Data are means ± SEM. ***p<0.001, ****p<0.0001 compared with vehicle-treated myotubes; #p<0.05, ##p<0.01, ###p<0.001 compared with control myotubes.

Table 1. Genotypes of CPT2 Patients

N°	Gender	Mutations
Patient 1	M	p.S113L/p.G377D
Patient 2	F	p.S113L/p.W201X
Patient 3	M	p.S113L/p.S38AfsX35
Patient 4	M	p.S113L/p.S113L

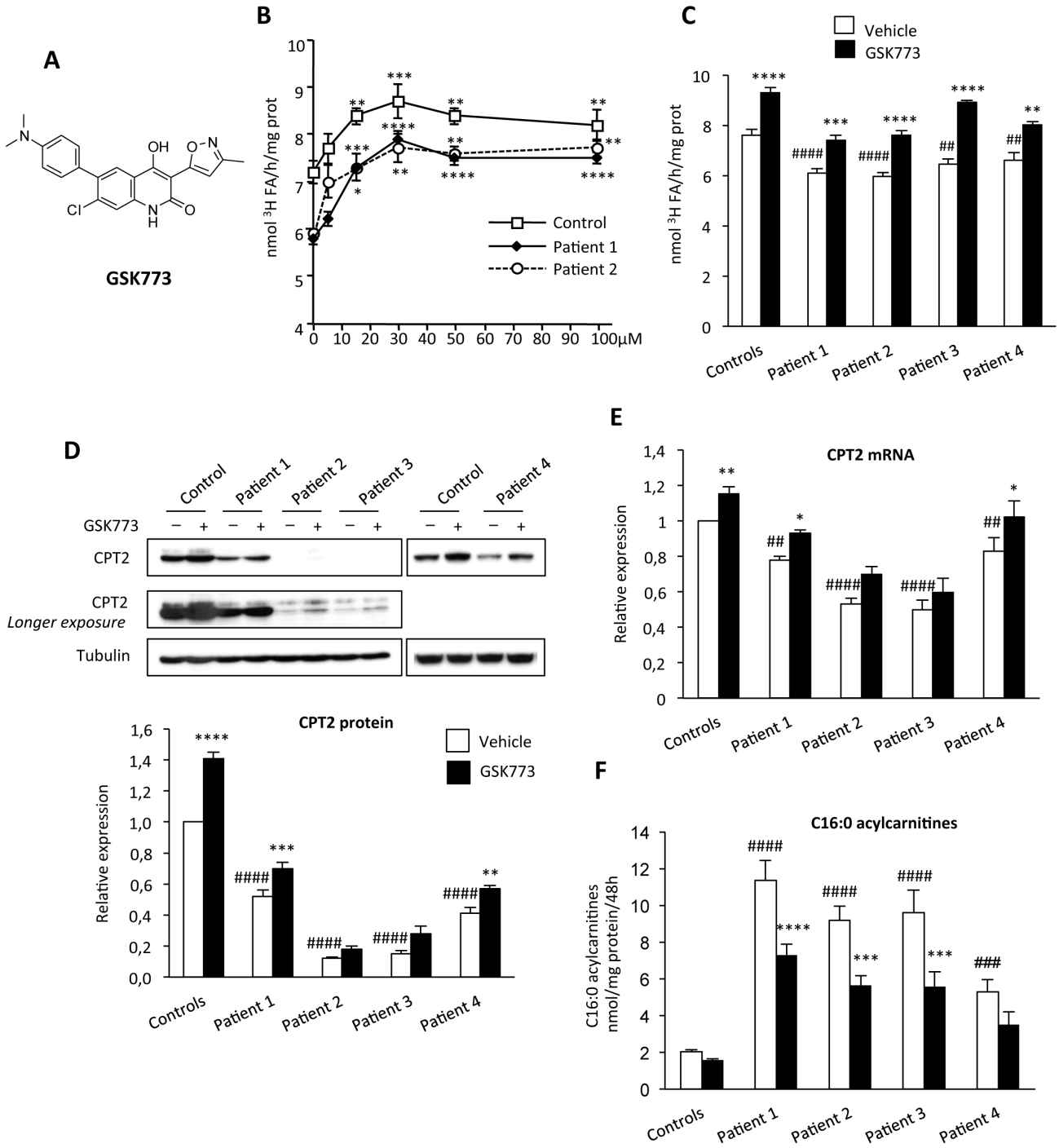
A
GSK773
B
nmol ³H FA/h/mg prot
Control
Patient 1
Patient 2
0 10 20 30 40 50 60 70 80 90 100µM
C
Vehicle
GSK773
nmol ³H FA/h/mg prot
Controls
Patient 1
Patient 2
Patient 3
Patient 4
D
Control
Patient 1
Patient 2
Patient 3
Control
Patient 4
GSK773
CPT2
CPT2
Longer exposure
Tubulin
CPT2 protein
Vehicle
GSK773
Relative expression
E
CPT2 mRNA
Relative expression
F
C16:0 acylcarnitines
C16:0 acylcarnitines
nmol/mg protein/48h

Figure 1

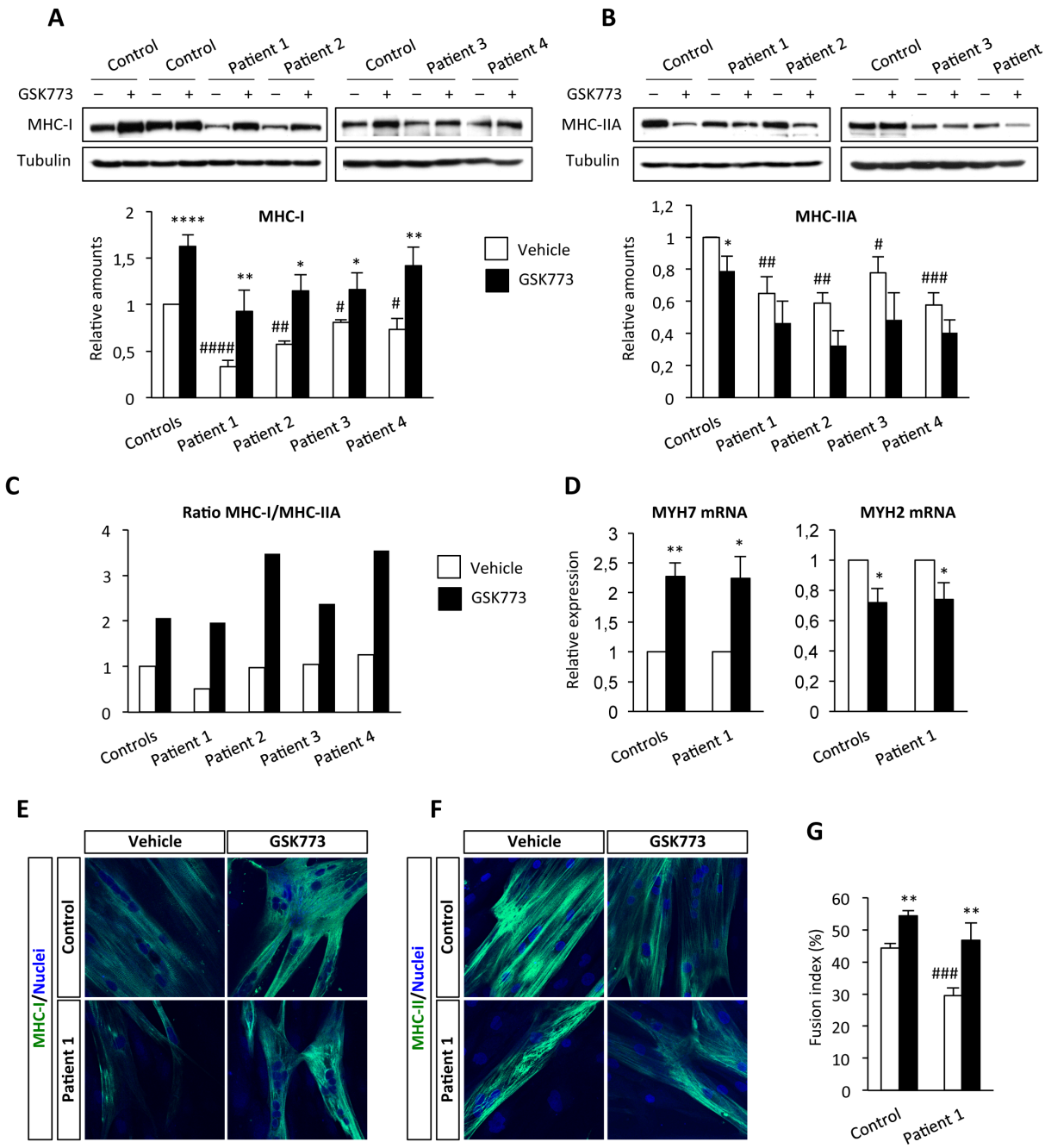
A
Control
Control
Patient 1
Patient 2
Control
Patient 3
Patient 4
GSK773
MHC-I
Tubulin
B
MHC-IIA
MHC-I
Relative amounts
Vehicle
GSK773
Controls
Patient 1
Patient 2
Patient 3
Patient 4
C
Ratio MHC-I/MHC-IIA
D
MYH7 mRNA
MYH2 mRNA
Relative expression
E
F
Vehicle
GSK773
MHC-I/Nuclei
MHC-II/Nuclei
Control
Patient 1
G
Fusion index (%)

Figure 2

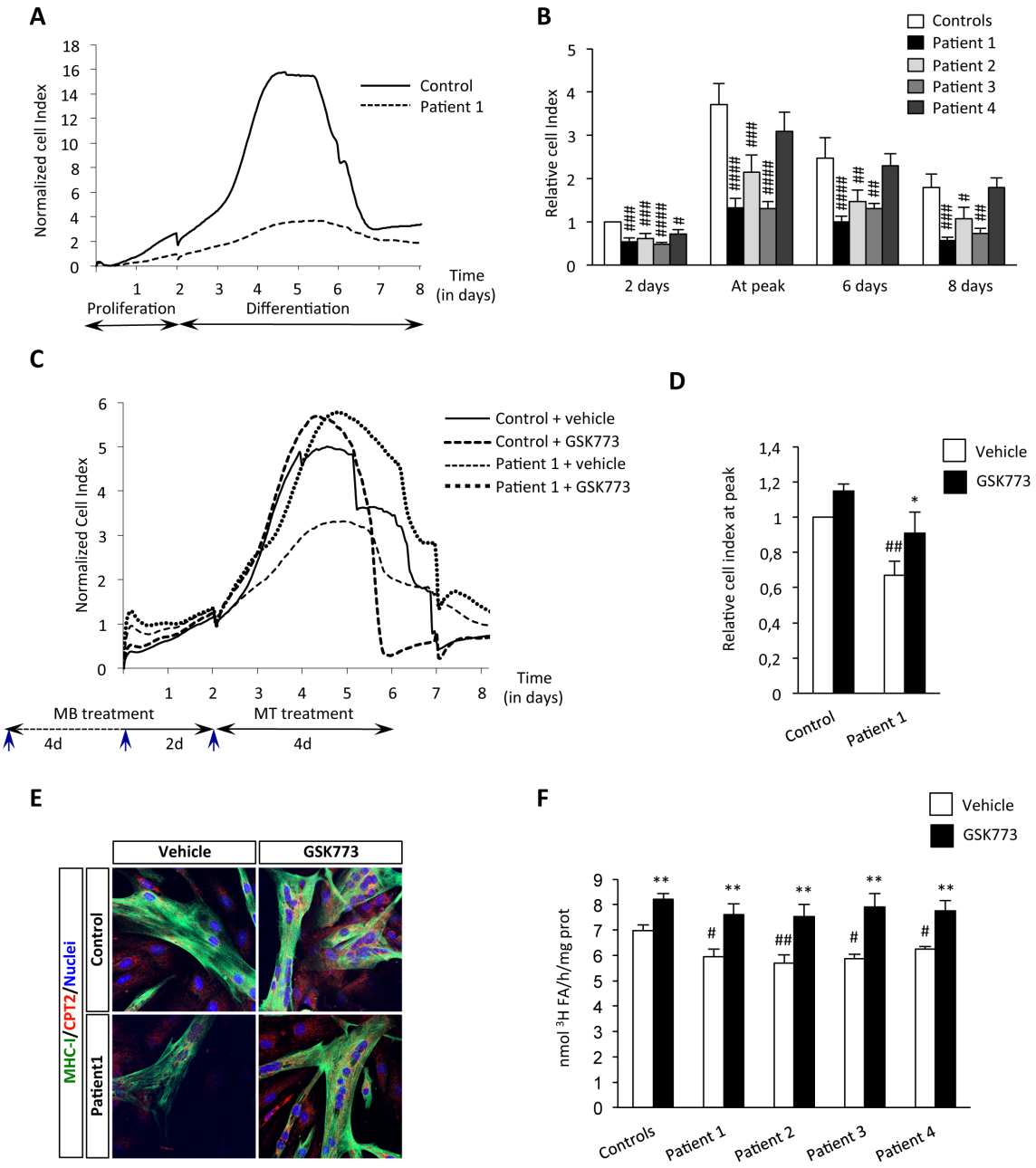
A
Normalized cell Index
Control
Patient 1
Time (in days)
Proliferation
Differentiation
B
Relative cell Index
Controls
Patient 1
Patient 2
Patient 3
Patient 4
2 days
At peak
6 days
8 days
C
Normalized Cell Index
Control + vehicle
Control + GSK773
Patient 1 + vehicle
Patient 1 + GSK773
Time (in days)
MB treatment
MT treatment
4d
2d
4d
D
Relative cell index at peak
Vehicle
GSK773
Control
Patient 1
E
Vehicle
GSK773
MHC-I/CPT2/Nuclei
Control
Patient1
F
Vehicle
GSK773
nmol ³H FA/h/mg prot
Controls
Patient 1
Patient 2
Patient 3
Patient 4

Figure 3

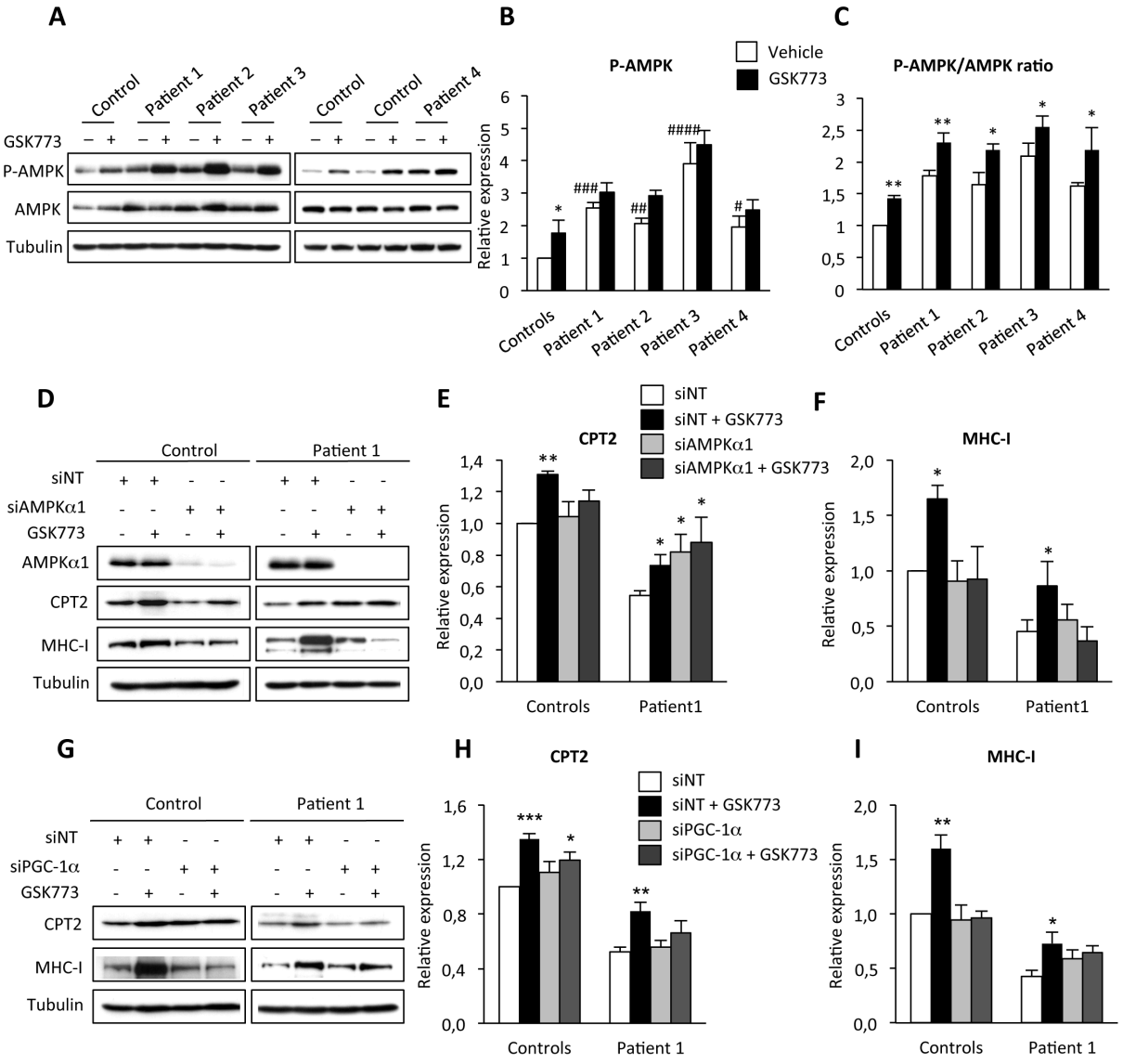
A
Control
Patient 1
Patient 2
Patient 3
Control
Control
Patient 4
GSK773
P-AMPK
AMPK
Tubulin
B
P-AMPK
Vehicle
GSK773
Relative expression
Controls
Patient 1
Patient 2
Patient 3
Patient 4
C
P-AMPK/AMPK ratio
Controls
Patient 1
Patient 2
Patient 3
Patient 4
D
Control
Patient 1
siNT
siAMPKα1
GSK773
AMPKα1
CPT2
MHC-I
Tubulin
E
CPT2
siNT
siNT + GSK773
siAMPKα1
siAMPKα1 + GSK773
Relative expression
Controls
Patient1
F
MHC-I
Relative expression
Controls
Patient1
G
Control
Patient 1
siNT
siPGC-1α
GSK773
CPT2
MHC-I
Tubulin
H
CPT2
siNT
siNT + GSK773
siPGC-1α
siPGC-1α + GSK773
Relative expression
Controls
Patient 1
I
MHC-I
Relative expression
Controls
Patient 1

Figure 4

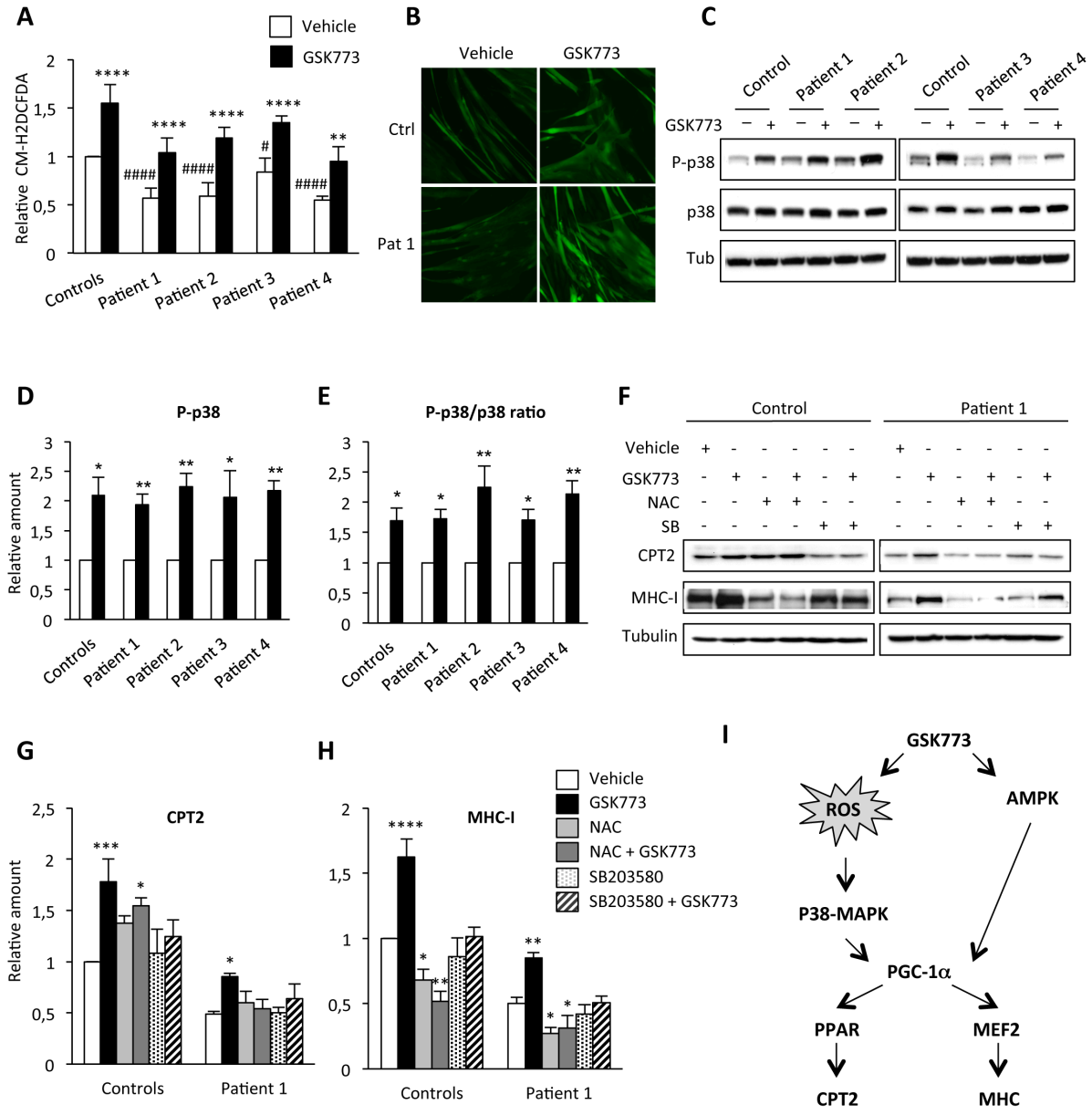
A
Vehicle
GSK773
Relative CM-H2DCFDA
Controls
Patient 1
Patient 2
Patient 3
Patient 4
B
Vehicle
GSK773
Ctrl
Pat 1
C
Control
Patient 1
Patient 2
Control
Patient 3
Patient 4
GSK773
P-p38
p38
Tub
D
P-p38
Relative amount
E
P-p38/p38 ratio
F
Control
Patient 1
Vehicle
GSK773
NAC
SB
CPT2
MHC-I
Tubulin
G
CPT2
Relative amount
H
MHC-I
Vehicle
GSK773
NAC
NAC + GSK773
SB203580
SB203580 + GSK773
I
GSK773
ROS
AMPK
P38-MAPK
PGC-1α
PPAR
MEF2
CPT2
MHC

Figure 5

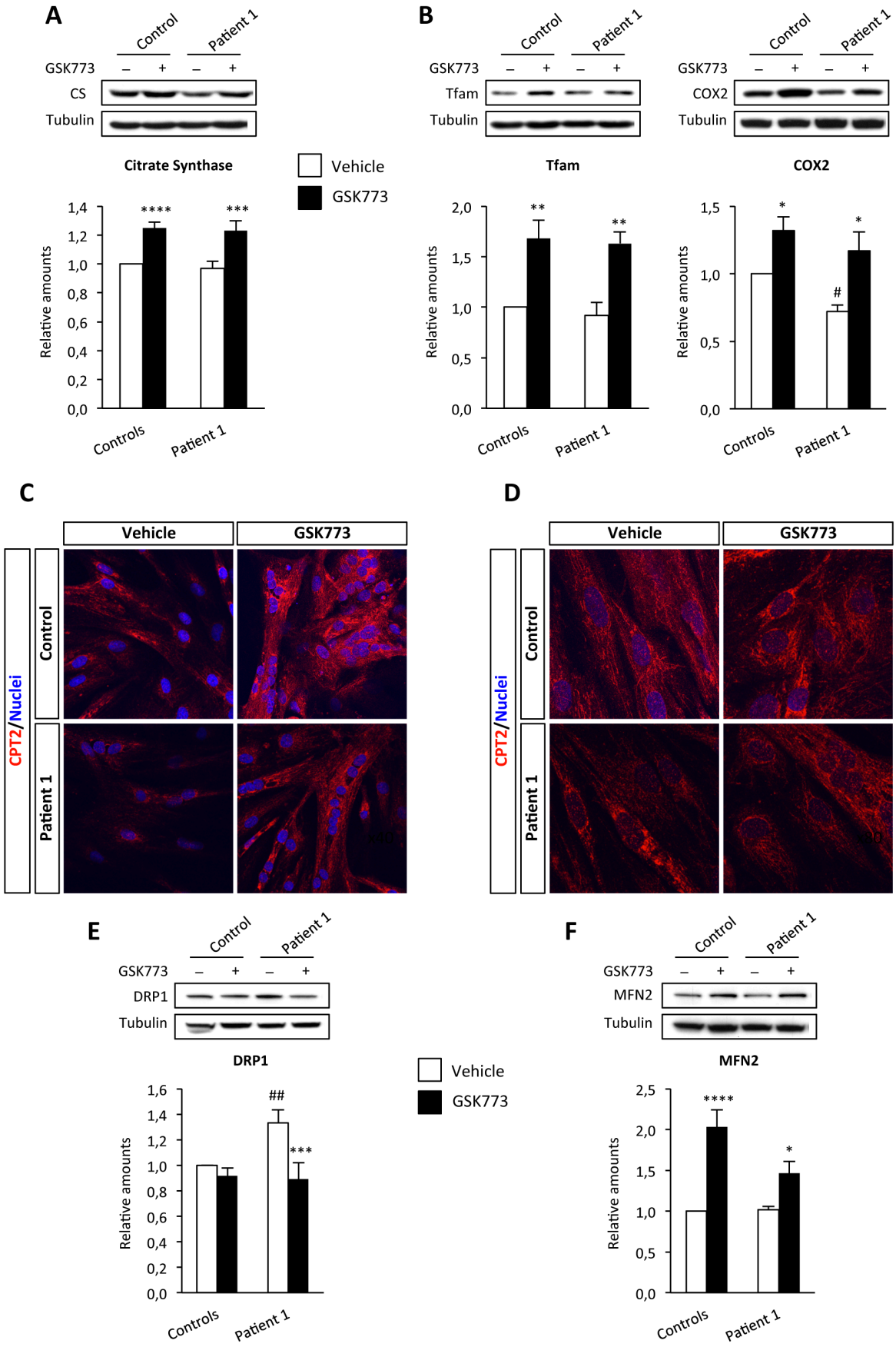
A
Control
Patient 1
GSK773
CS
Tubulin
Citrate Synthase
Vehicle
GSK773
Relative amounts
Controls
Patient 1
B
Tfam
COX2
C
D
Vehicle
GSK773
CPT2/Nuclei
Control
Patient 1
E
DRP1
F
MFN2

Figure 6

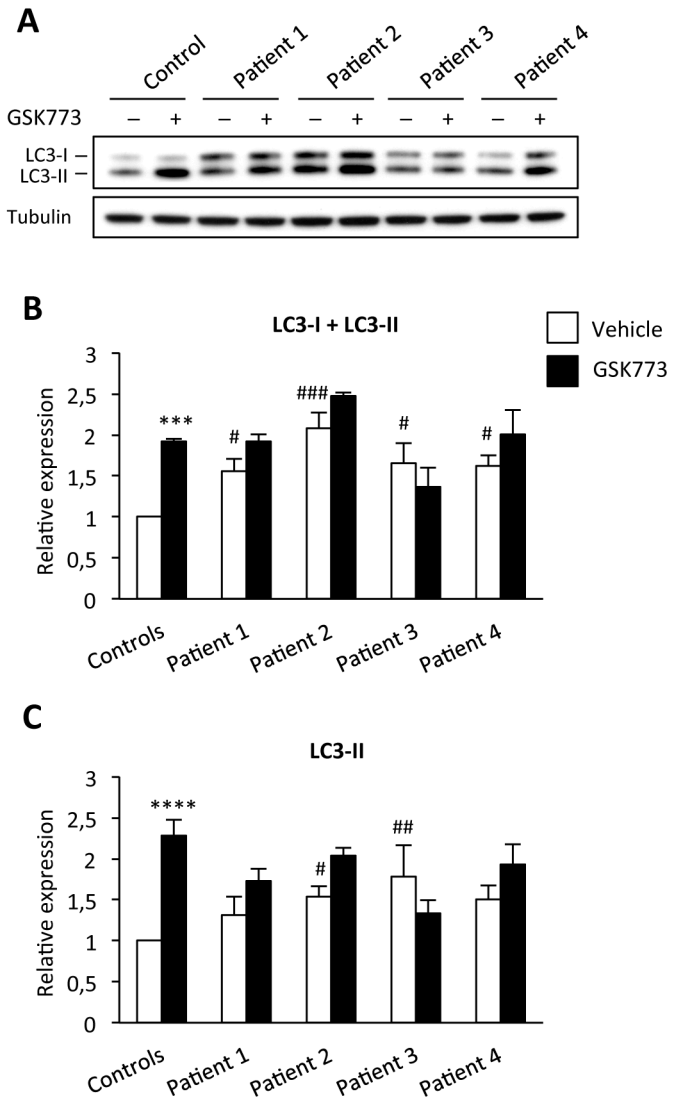
A
Control
Patient 1
Patient 2
Patient 3
Patient 4
GSK773
– + – + – + – + – +
LC3-I
LC3-II
Tubulin
B
LC3-I + LC3-II
Vehicle
GSK773
Relative expression
3
2,5
2
1,5
1
0,5
0
***
#
###
#
#
Controls
Patient 1
Patient 2
Patient 3
Patient 4
C
LC3-II
Relative expression
****
#
##
Controls
Patient 1
Patient 2
Patient 3
Patient 4

Figure 7

A

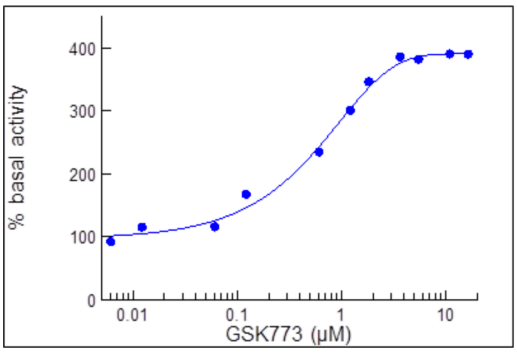

B

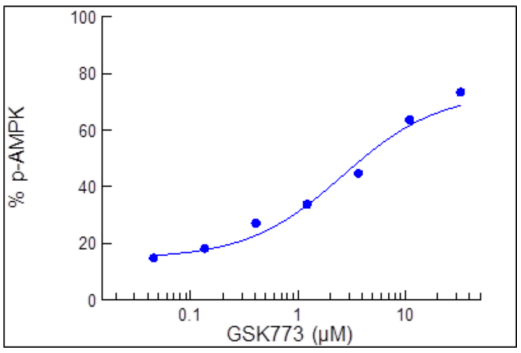

C

AMPK trimer	EC_{50} (μM)
α1β1γ1	0.08
α2β1γ1	0.02
α1β1γ2	0.13
α1β1γ3	0.10
α1β2γ1	>30
α2β2γ1	>30
α2β2γ3	>30

D

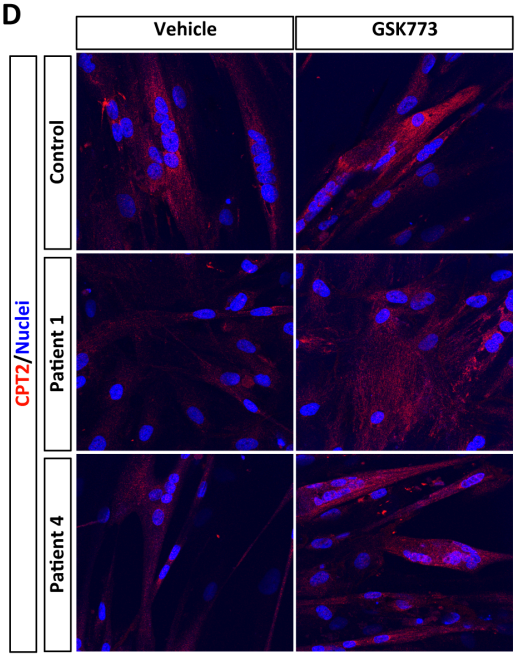

Figure S1. GSK773 is a direct and specific activator of AMPK, Related to figure 1

(A) GSK773 stimulates partially purified rat liver AMPK (EC50 ~ 1μM). Activity was monitored by measuring ^{33}P-phosphorylation of the SAMS peptide substrate, a widely used substrate for AMPK.

(B) GSK773 protects rat liver AMPK from de-phosphorylation (EC50 ~ 3μM).

(C) GSK773 is a β1 selective AMPK direct activator. Activity was monitored by AMPK FRET-based assay (Z'-LYTE) using human recombinant AMPK heterotrimers.

(D) GSK773 stimulates CPT2 protein level (in red).

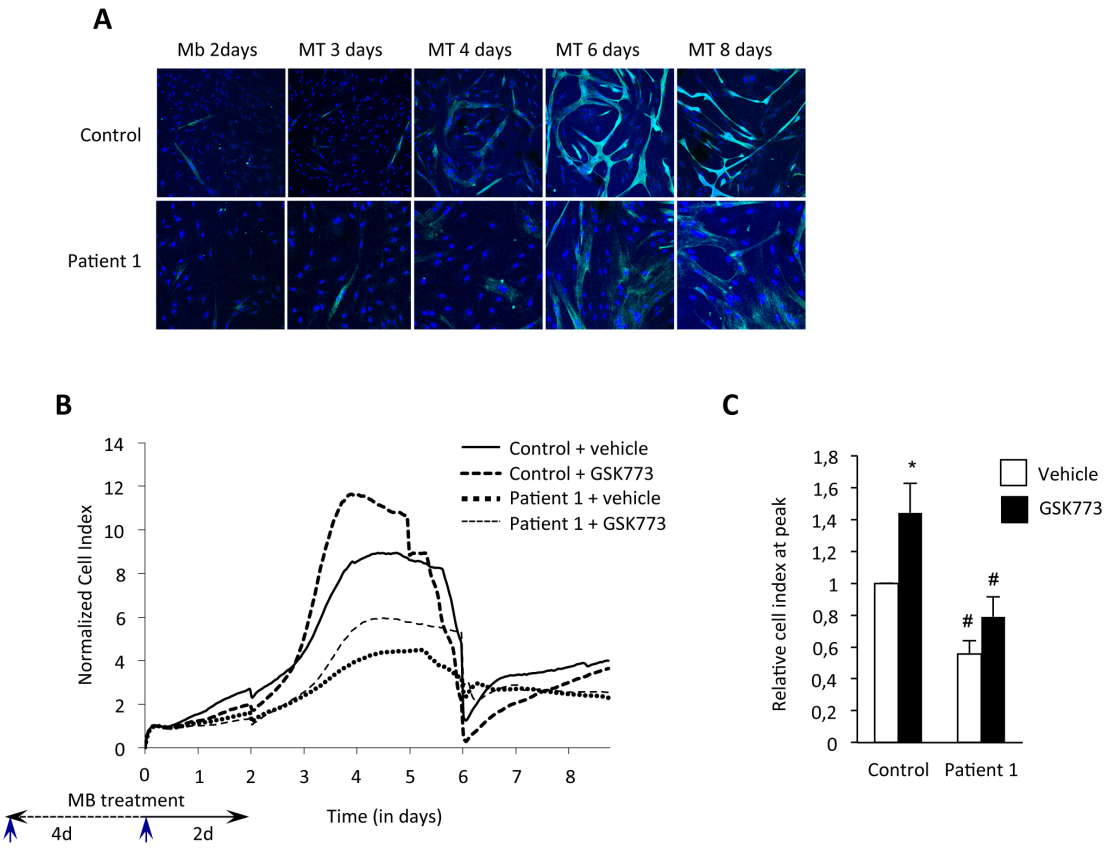

Figure S2. Related to figure 3

(A) Representative immunofluorescence images of untreated myoblast (MB) and myotubes (MT) at different times of the kinetic: MHC-I (green) and Topro-3-labeled nuclei (blue).

(B) Representative kinetics of muscle cells treated with 30µM GSK773 for 6 days during myoblasts' proliferation. The blue arrows represent the treatments.

(C) Maximum cell index of myoblasts treated for 6 days; (n=3 experiments).

Data are means ± SEM. *p<0.05 *versus* vehicle-treated myotubes; #p<0.05 versus vehicle-treated control myotubes.

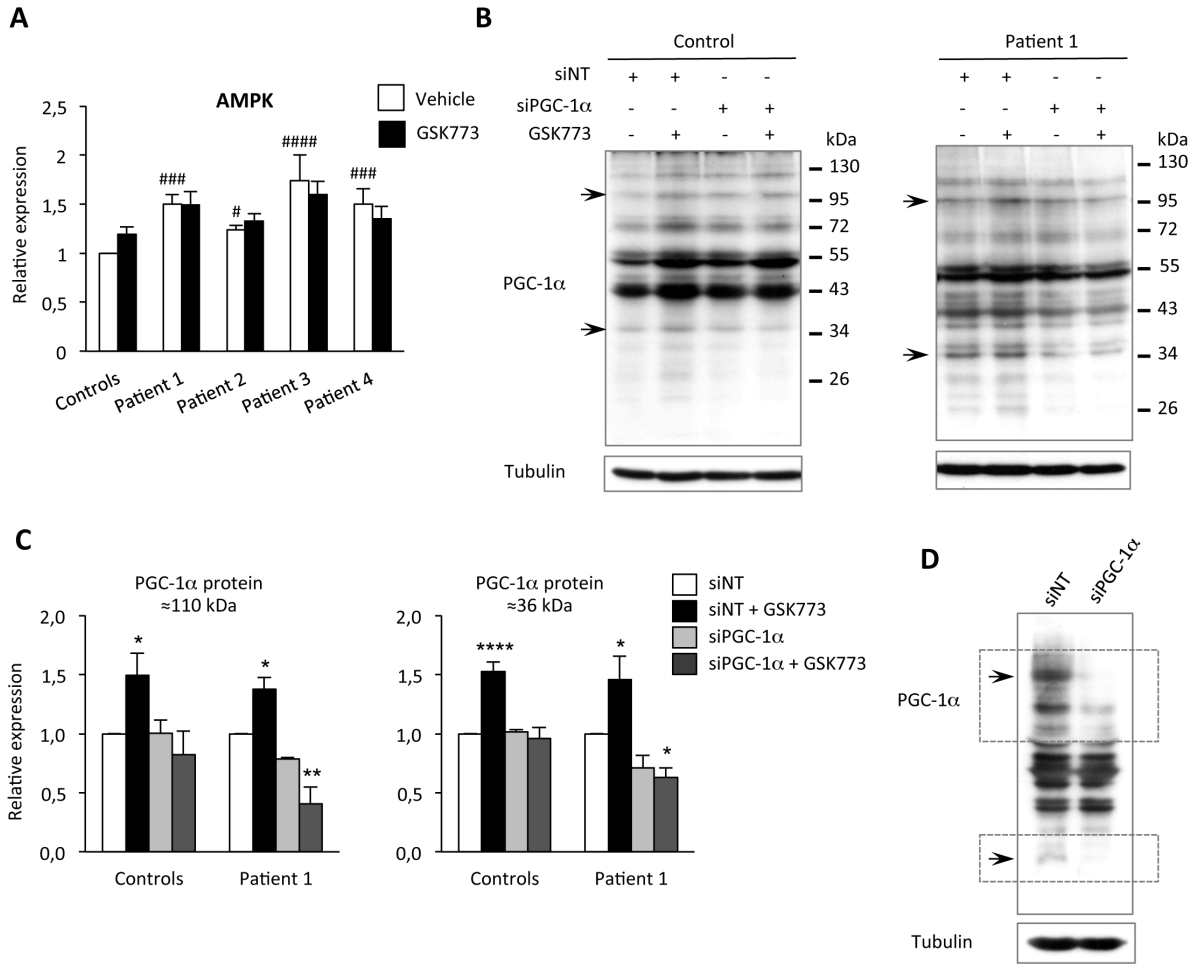

Figure S3. Related to figure 4

(A) Quantification of AMPK protein levels in myotubes (30 µM GSK773, 48h).

(B) Representative western blots of PGC-1α. According to our protocol, myotubes were induced to differentiate two days and then transfected with siNon-target (NT) or siPGC-1α. Two days after transfection, the myotubes were treated with 30 µM GSK773 for 48h (n= 5 independent experiments). The arrows indicate the bands that were quantified.

(C) Quantification of the ≈110 kDa and the ≈36 kDa PGC-1α proteins.

(D). Representative western blots of PGC-1α. Myotubes were transfected, with siNon-target (NT) or siPGC-1α, two days after induction of differentiation. Cell extracts were performed 2 days after transfection, which normally corresponds to the day when the myotubes were treated.

Data are means ± SEM. #p<0.05, ###p<0.001, ####p<0.0001 compared with control myotubes.

*p<0.05, **p<0.01, ****p<0.0001 versus vehicle-treated myotubes.

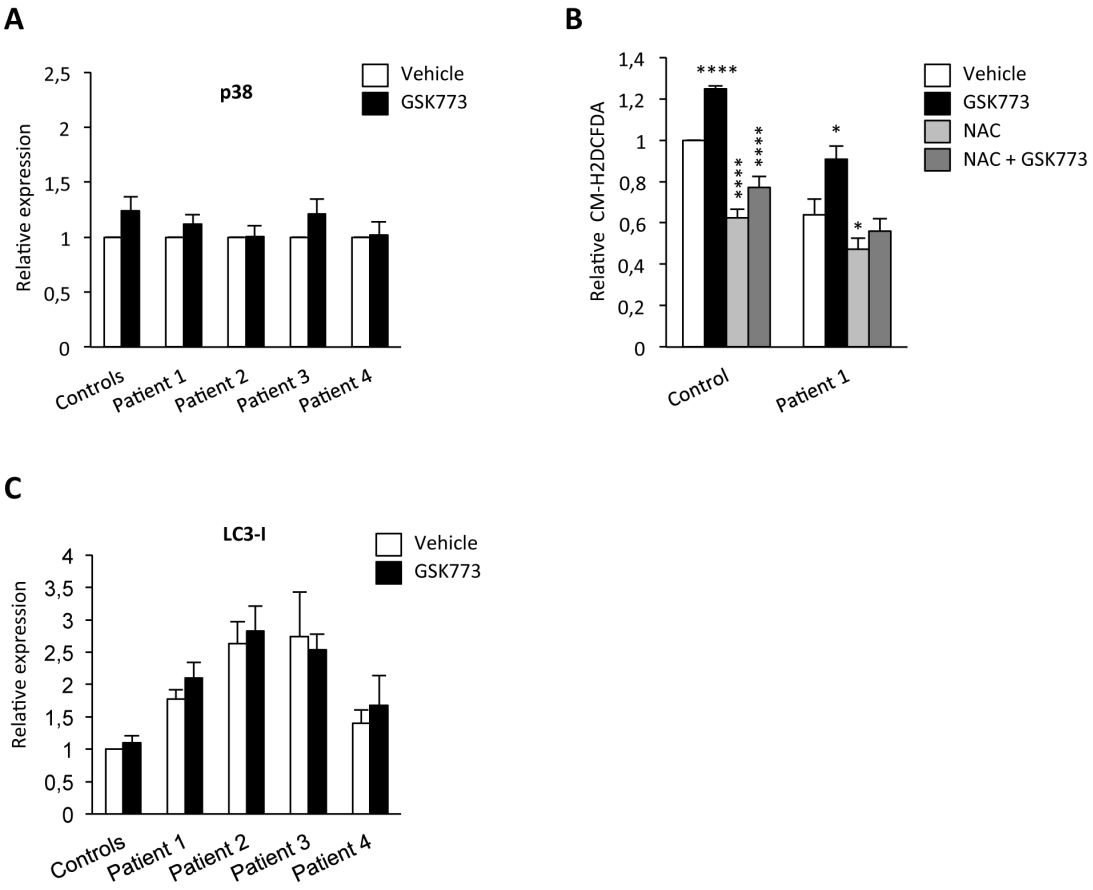

Figure S4. Related to figure 5 and 7

(A) Quantification of p38 protein levels in myotubes (30 µM GSK773, 48h); (n=3 different experiments).

(B) Relative measurement of total ROS production in myotubes after 1h of treatment with 30µM GSK773 in conjunction with 10mM NAC (n=3 independent experiments).

(C) Quantification of LC3-I protein levels in myotubes (30 µM GSK773, 48h); (n=3 different experiments).

Data are means ± SEM. *p<0.05, **p<0.01, ***p<0.001, ****p<0.0001 compared with vehicle-treated myotubes.